

Complement downregulation promotes an inflammatory signature that renders colorectal cancer susceptible to immunotherapy

Carsten Krieg,^{1,2} Lukas M Weber,^{3,4} Bruno Fosso,⁵ Marinella Marzano ⁵, Gary Hardiman,⁶ Monica M Olcina,⁷ Enric Domingo ⁷, Sahar El Aidy,⁸ Khalil Mallah,⁹ Mark D Robinson,^{3,4} Silvia Guglietta ^{2,10,11}

To cite: Krieg C, Weber LM, Fosso B, *et al.* Complement downregulation promotes an inflammatory signature that renders colorectal cancer susceptible to immunotherapy. *Journal for ImmunoTherapy of Cancer* 2022;**10**:e004717. doi:10.1136/jitc-2022-004717

► Additional supplemental material is published online only. To view, please visit the journal online (<http://dx.doi.org/10.1136/jitc-2022-004717>).

Accepted 29 August 2022

ABSTRACT

Background and aims The role of inflammatory immune responses in colorectal cancer (CRC) development and response to therapy is a matter of intense debate. While inflammation is a known driver of CRC, inflammatory immune infiltrates are a positive prognostic factor in CRC and predispose to response to immune checkpoint blockade (ICB) therapy. Unfortunately, over 85% of CRC cases are primarily unresponsive to ICB due to the absence of an immune infiltrate, and even the cases that show an initial immune infiltration can become refractory to ICB. The identification of therapy supportive immune responses in the field has been partially hindered by the sparsity of suitable mouse models to recapitulate the human disease. In this study, we aimed to understand how the dysregulation of the complement anaphylatoxin C3a receptor (C3aR), observed in subsets of patients with CRC, affects the immune responses, the development of CRC, and response to ICB therapy.

Methods We use a comprehensive approach encompassing analysis of publicly available human CRC datasets, inflammation-driven and newly generated spontaneous mouse models of CRC, and multiplatform high-dimensional analysis of immune responses using microbiota sequencing, RNA sequencing, and mass cytometry.

Results We found that patients' regulation of the complement C3aR is associated with epigenetic modifications. Specifically, downregulation of *C3ar1* in human CRC promotes a tumor microenvironment characterized by the accumulation of innate and adaptive immune cells that support antitumor immunity. In addition, in vivo studies in our newly generated mouse model revealed that the lack of C3a in the colon activates a microbiota-mediated proinflammatory program which promotes the development of tumors with an immune signature that renders them responsive to the ICB therapy.

Conclusions Our findings reveal that C3aR may act as a previously unrecognized checkpoint to enhance antitumor immunity in CRC. C3aR can thus be exploited to overcome ICB resistance in a larger group of patients with CRC.

WHAT IS ALREADY KNOWN ON THIS TOPIC

⇒ The presence of an inflammatory immune infiltrate in colorectal cancer (CRC) is a positive prognostic marker and can confer susceptibility to immune checkpoint blockade therapy. Despite the inflammatory nature of the majority of CRC, only a minority of these cancers are currently amenable to immunotherapy and often develop resistance. This raises the question whether additional mechanisms associated with tumor development can be exploited to enhance the efficacy of immunotherapy and extend its application to a larger number of patients with CRC.

WHAT THIS STUDY ADDS

⇒ In this study, we found that the complement anaphylatoxin C3a receptor (C3aR) is downregulated in human CRC. Patients with C3aR downregulation show enhanced infiltration with innate and adaptive activated immune cells. Our in vivo studies demonstrate that the loss of C3aR in a novel spontaneous model of CRC promotes the development of a microbiota-dependent inflammatory signature in typically cold tumor and makes them responsive to immunotherapy.

⇒ As such, our study unravels a previously unrecognized role of C3aR as an immune checkpoint in CRC, which could be exploited to enhance antitumor immunity and potentially extend immunotherapy to a larger number of patients with CRC.

INTRODUCTION

Inflammation in colorectal cancer (CRC) is a double-edged sword as inflammatory immune responses can either promote tumor development and progression or be exploited for therapy. On the one hand, independently of the nature of the tumors, sporadic or genetic, inflammation is a well-known driver of CRC development¹: about 20% of individuals with persistent gastrointestinal inflammation,



© Author(s) (or their employer(s)) 2022. Re-use permitted under CC BY-NC. No commercial re-use. See rights and permissions. Published by BMJ.

For numbered affiliations see end of article.

Correspondence to

Dr Silvia Guglietta;
guglietta@muscc.edu

such as patients with inflammatory bowel disease, develop CRC, and in sporadic CRC, the sequential accumulation of genetic alterations in tumor suppressors and oncogenes supports the development of an intrinsic inflammatory gene signature.^{2,3} On the other hand, the notion that immunosurveillance and associated immune responses can also be exploited for treatment is supported by the observation that Crohn's-like lymphoid infiltrates are a positive prognostic factor in patients with CRC.⁴ However, despite the inflammatory nature of most CRCs, since the introduction of immunotherapy with immune checkpoint blockade (ICB), only a minority of CRC proved to be amenable to this treatment.^{5,6}

To date, the Food and Drug Administration has granted approval of CRC to ICB with anti-programmed cell death-1 (PD-1) alone or in combination with anti-cytotoxic T-lymphocyte-associated protein 4 (CTLA-4) only in patients with microsatellite unstable high CRC (MSI-H CRC), which represent 15% of all CRC and 5% of metastatic CRC.⁷ Most importantly, independently of the PD-L1 expression, BRAF, KRAS mutations, and Lynch syndrome status, over 50% of MSI-H CRCs do not respond or develop resistance to ICB.⁸ Further, approximately 21% of patients with microsatellite stable (MSS) CRC show an immune signature similar to MSI-H CRC, which may render them susceptible to ICB.⁹ Therefore, while it is evident that there can be a favorable and an unfavorable inflammation in CRC, identifying the underlying mechanisms that determine one or the other to broaden ICB responsiveness requires a deeper understanding of the events associated with CRC development.

Alterations in innate sensing mechanisms play a crucial role in intestinal inflammation and CRC.¹⁰ The complement system is a central player because it can establish extensive networks with other innate immune and adaptive pathways.^{11,12} We previously reported that activation of the alternative complement pathway C3a–C3a receptor (C3aR) during spontaneous small intestinal tumorigenesis is involved in tumor-associated thrombosis via the promotion of neutrophil extracellular trap (NET) formation.¹³ Furthermore, in an intestinal ischemia/reperfusion injury model, the C3a–C3aR axis proved essential for tissue regeneration and protection from oxidative damage.¹⁴ These findings suggest a critical function for the C3a–C3aR axis in intestinal homeostasis, but its role in CRC remains understudied.

In the present study, by mining publicly available datasets, we found that *C3ar1* gene methylation and downregulation of the C3aR expression occur in subsets of human CRC independently of their MSI or MSS status. We also found that in patients, reduced levels of C3aR expression correlate with increased accumulation in the tumor microenvironment (TME) of innate and adaptive immune responses, which support antitumor immunity. When generating a new in vivo mouse model, we found that APC^{Min/+} mice, which usually develop tumors almost exclusively in the small intestine, mainly developed tumors in the colon. The TME analysis revealed

that colon tumors originating in the absence of C3aR signaling showed marked innate and adaptive immune infiltrates with prominent Th1, Th17, and cytotoxic T-cell signatures. Both immune infiltration and tumor development in the colon of APC^{Min/+}/C3aR^{-/-} mice could be recapitulated in APC^{Min/+} mice by fecal microbiota transplantation (FMT) experiments. Finally, we showed that the absence of C3aR treatment with anti-PD-1 effectively reduced tumor growth in otherwise ICB unresponsive APC^{Min/+} tumors, therefore demonstrating that the inflammatory infiltrate induced by loss or downregulation C3aR in CRC can be successfully exploited to enhance response to therapy.

Altogether our data indicate that loss or downregulation of C3aR could represent the Achilles's heel of CRC by rendering cold tumor hot and serve as a previously unexplored additional immune checkpoint in CRC.

MATERIALS AND METHODS

Extended materials and methods can be found in the online supplemental information.

Animals

C57BL/6J-ApcMin/J (referred to as APC^{Min/+}), C57BL/6J (referred to as WT), C3aR^{-/-} and APC^{Min/+}/C3aR^{-/-} mice were bred and maintained in our specific pathogen free (SPF) animal facility at the European Institute of Oncology and the Medical University of South Carolina. Animal Research Reporting of In Vivo Experiments (ARRIVE) guidelines were used.¹⁵

CRC models

For inflammation-driven CRC, mice were treated with azoxymethane (AOM, Sigma-Aldrich) and dextran sulfate sodium (DSS) as previously described.¹⁶ For the spontaneous tumor model, APC^{Min/+} and APC^{Min/+}/C3aR^{-/-} mice were euthanized at the indicated time points, tumor counted, and used for downstream applications.

Flow cytometry and preparation of single-cell suspensions

Single-cell suspensions were prepared from mLN following standard protocols. In addition, colon lamina propria (cLP) and tumor cells were isolated as previously described with minor modifications.¹⁷ Protocols for the generation of single-cell suspensions and antibodies used can be found in the online supplemental information. Samples were acquired with FACSCanto II or Fortessa LSR (BD Bioscience) and analyzed with FlowJo software (TreeStar).

Fecal microbiota transplantation

For FMT, fecal material was obtained from APC^{Min/+} and APC^{Min/+}/C3aR^{-/-} donor mice. Fecal pellets and cecal contents were harvested and frozen in Columbia broth with 20% glycerol. At the administration time, aliquots were thawed, centrifuged to eliminate the glycerol-containing medium, and gavaged. This procedure allowed us to use the same material throughout the

experiment, avoiding confounding effects due to fecal material coming from different animals.

Microbiota profiling

V5–V6 hypervariable regions of bacterial 16S rRNA gene were amplified and processed with a modified version of the Nextera protocol.¹⁸ The obtained metabarcoding libraries were sequenced using the MiSeq Illumina platform. In addition, metagenomic amplicons were analyzed by applying the BioMaS¹⁹ pipeline.

RNA sequencing (RNA-Seq) and RNA-Seq data analysis using the edgeR framework

According to manufacturer instructions, the proximal and distal colon and the single tumors were immediately preserved in RNAlater stabilization solution (Qiagen) and stored at -20°C . For RNA extraction, tumors and colons were homogenized in Trizol. The supernatant was loaded on Qiagen Mini Kit columns and treated as indicated in the manufacturer instructions. RNA was quantified at the Nanodrop and used to generate libraries using the TruSeq RNA kit (Illumina). Quality and integrity of the obtained libraries were evaluated using a bioanalyzer (Agilent Technologies). Samples were sequenced on an Illumina MiSeq instrument at a depth of 35×10^6 reads per sample.

All analyses were performed using the R environment for statistical computing (R V.3.3.1) using Bioconductor Release V.3.3 as well as other packages.²⁰ Alignment to the mouse reference genome (GRCm38.82) was performed using STAR V.2.5.0a followed by gene-level counting using the featureCounts function of the Rsubread package V.1.22.3.²¹ Raw counts were normalized using edgeR V.3.14.0, and differential expression was determined using generalized linear models and likelihood ratio tests from the edgeR package.^{22,23} Significance was determined using the edgeR function `decideTestsDGE` with Benjamini-Hochberg correction for false discovery rate (FDR); a default FDR threshold of 0.05 and a log2 fold change threshold of 0.6 were applied. Gene set enrichment analyses were conducted using the camera function in the limma package V.3.28.21.²⁴

Analysis of C3aR expression, methylation and correlation with immune cells in patients with rectal and colon cancers

Data on C3aR expression were obtained from the R2 Genomics Analysis and Visualization Platform (<http://r2.amc.nl>) or TCGA database. Data on C3aR methylation were obtained from the human pan-cancer methylation database (<http://methhc.mbc.nctu.edu.tw/php/index.php>).²⁵ The correlations of C3aR expression and immune cells on a retrospective cohort of 231 patients with rectal cancer in the S:CORT WS3 Grampian Set and 97 patients with colon cancer in the FOxTROT cohort were visualized and downloaded through the private S:CORT cBioPortal. The data deconvolution was performed using CIBERSORT, xCell, and MCP.

Mass cytometry

Mass cytometry antibodies were either labeled in-house using antibody-labeling kits and protocols or purchased from Fluidigm according to the manufacturer's instructions. For live-cell barcoding, we followed the protocol by Mei *et al.*²⁶ using six metal isotopes and adapted it to live-cell barcoding of samples with CD45.2 following the protocol published by Lai *et al.*²⁷ Briefly, individual samples were incubated with unique choose three out of six CD45–platinum or CD45–indium barcodes (table 1) in cell staining buffer for 15 min at 4°C , washed twice, and combined into one composite sample. To identify dead cells, 2.5 μM live/dead marker Pt198 in phosphate-buffered saline (PBS) was added for 2 min at RT. After washing, the composite sample was stained with the cocktail of primary antibodies as described in the online supplemental information. Data from different days and across acquisition time were normalized by adding five-element beads to the sample immediately before acquisition and using the MATLAB-based normalization software, as described previously.²⁸

Statistical analysis

Data were analyzed for normal distribution before performing statistical analyses. Values are presented as means \pm SEM of multiple individual experiments, each carried out at least in duplicate or as means \pm SEM of replicates in a representative experiment. Student's t-test determined a comparison between two groups. Comparison of multiple groups was carried out by one-way or two-way analysis of variance followed by Bonferroni post-test correction using GraphPad Prism software V.8 as indicated in the figure legends. All statistical tests were two-sided, and $p < 0.05$ was considered statistically significant unless otherwise specified.

RESULTS

c3ar1 downregulation occurs in patients with CRC

The analysis of the gene expression libraries provided through the Skrzypczack Colorectal cohort, Sabates-Bellver Colon cohort, Ki Colon cohort, and the Cancer Genome Atlas (TCGA) cohort (<https://www.oncomine.org>) revealed that downregulation of C3aR occurs in patients with CRC compared with controls (figure 1A). We found that C3aR downregulation occurred in approximately 33% of patients with MSI-H CRC and 34% of patients with MSS CRC. Additionally, although patients with stages II and III showed significantly lower expression than stage I patients, overall, the reduction in C3aR expression was not specific for a defined tumor stage (online supplemental figure 1). Since mutations of single genes in the complement pathway are rare, we reasoned that downregulation of the *c3ar1* gene might be mediated by epigenetic modifications.²⁹ Methylation occurs at a high frequency in CRC.³⁰ We mined the MethHC database of DNA methylation and gene expression in human cancer and found that the *c3ar1* gene is highly methylated in CRC

Table 1 Cytometry by time of flight (CyTOF) barcodes and antibodies

Antigen	Mass	Metal conjugate	Clone	Vendor	Comment
Technical channels					
Nucleic acid intercalator	198	Pt	NA	Fluidigm	Live-dead
DNA-1	191	Ir	NA	Fluidigm	Nuclear DNA
DNA-2	193	Ir	NA	Fluidigm	Nuclear DNA
BC105	105	Pt	104.2	BioXcell	All hematopoietic cells except mature erythrocytes and platelets
BC113	113	In	104.2	BioXcell	All hematopoietic cells except mature erythrocytes and platelets
BC115	115	In	104.2	BioXcell	All hematopoietic cells except mature erythrocytes and platelets
BC194	194	Pt	104.2	BioXcell	All hematopoietic cells except mature erythrocytes and platelets
BC195	195	Pt	104.2	BioXcell	All hematopoietic cells except mature erythrocytes and platelets
BC196	196	Pt	104.2	BioXcell	All hematopoietic cells except mature erythrocytes and platelets
Cell-type markers					
Ly6G	141	Pr	1A8	Fluidigm	Granulocytes, macrophages/monocytes
CD11c	142	Nd	N418	Fluidigm	T cells, DCs, NK cells, stem cells/progenitors, macrophages/monocytes, granulocytes
CD11b	143	Nd	M1/70	Fluidigm	DCs, NK cells, macrophages/monocytes
CD4	145	Nd	RM-4-5	Fluidigm	T cells, DCs, NK cells, stem cells/progenitors, macrophages/monocytes
CD19	149	Sm	6D5	Fluidigm	B cells, DCs, stem cell/progenitors
Ly6C	150	Nd	HK1.4	Fluidigm	Macrophages, monocytes, neutrophils, T cells
CD3	152	Sm	145-2C11	Fluidigm	NKT cells, T cells, thymocytes
NK1.1	155	Gd	PK136	Fluidigm	NK cells, NKT cells, NKp22 cells
CD8	168	Er	53-6.7	Fluidigm	Most thymocytes, T-cell subset, some NK cells, lymphoid DCs
CD44	171	Yb	IM7	Fluidigm	B cells, leukocytes, Tregs, T-cell memory
MHC 2 - I-A/I-E	174	Yb	M5/114.15.2	Fluidigm	Antigen-presenting cells, B cells, DCs, T cells, Tregs
Cell state markers and intracellular functional markers					
IL-2	144	Nd	JES65H4	Fluidigm	T cells
IL-12p70	156	Gd	C18.2	eBioscience	B lymphocytes, DCs, and macrophages, ILC1
Foxp3	158	Gd	FJK16s	Fluidigm	Regulatory T cells
IL-22	160	Gd	Poly5164	ThermoFisher	Th17, Th1, Th2, lymphoid tissue inducer cells, and subsets of natural killer cells, ILC
TNF- α	162	Dy	MP6XT22	ThermoFisher	Activated monocytes, neutrophils, macrophages, T cells, B cells, NK cells, LAK cells
IL-17	165	Ho	TC11-18H10	BioLegend	CD4 memory T cells, ILC3
IL-4	166	Er	11B11	Fluidigm	Mast cells, T cells, bone marrow stromal cells, ILC2
IL-6	167	Er	MP520F3	Fluidigm	T cells, B cells, macrophages, bone marrow stromal cells
IFN- γ	176	Yb	XMG1.2	ThermoFisher	T cells, NK cells, ILC1

Source: BD CD Marker Handbook, BioLegend.

DC, dendritic cell; IFN- γ , interferon gamma; IL, interleukin; NK, natural killer; TNF- α , tumor necrosis factor alpha.

tissues compared with normal mucosa.²⁵ Remarkably, we found significant hypermethylation in the N and S shores (regions up to 2 kb away from CpG islands) and in the shelves (figure 1B–D), which, as shown by Irizarry and collaborators, inversely correlates with gene expression levels.³¹ These results suggest that the downregulation of C3aR in CRC may be driven by CpG island methylation events, which are prominent for CRC development.³² These novel findings suggest that C3aR plays an important role in the human intestinal tract. In support of this hypothesis, loss or reduction of C3aR caused by DNA methylation events, as

we reported in patients, may favor the establishment of CRC.

C3a–C3aR axis plays a previously unappreciated role in CRC development

To test the role of the C3a–C3aR axis in CRC development, we reverse-translated our findings from the database and investigated CRC development in vivo in mice lacking C3aR. First, age-matched and sex-matched C3aR^{−/−} and WT mice were administered the carcinogen AOM followed by three cycles of the inflammatory agent DSS. Relative to WT, C3aR^{−/−} mice showed increased

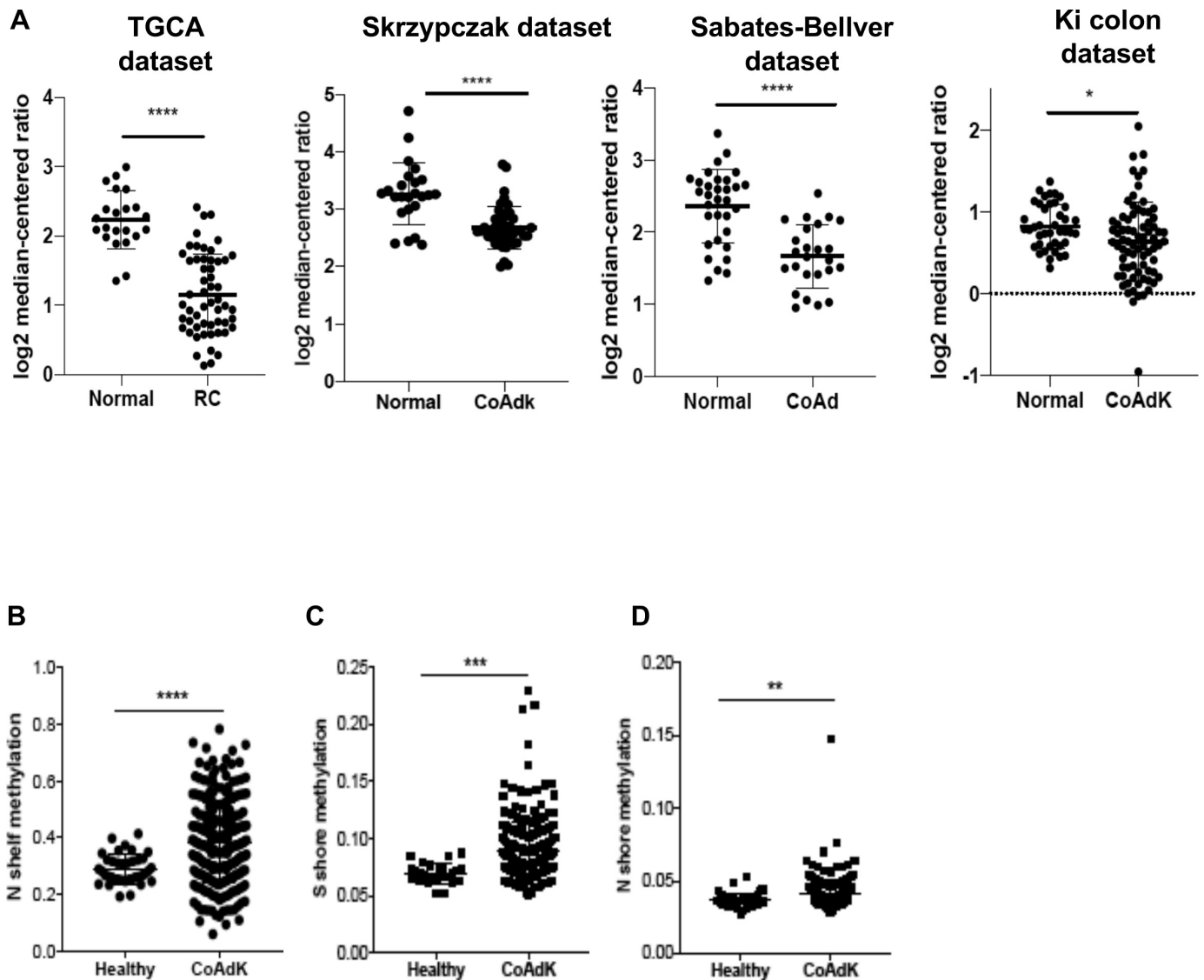


Figure 1 C3aR methylation and downregulation in patients with CRC. (A) C3aR expression in patients with RC and colon cancer from four independent datasets (TGCA: 22 healthy, 55 RC; Skrzypczak cohort: 24 healthy, 45 CoAdK; Sabates-Bellver cohort: 32 healthy, 25 CoAd; Ki cohort: 41 healthy, 76 CoAdK). (B) N shelf, (C) S shore and (D) N shore methylation of *c3ar1* in patients with CRC. Significance was calculated using t-test. * $P > 0.05$, ****= $P > 0.0001$. C3aR, C3a receptor; CoAd, colon adenoma; CoAdK, colon adenocarcinoma; CRC, colorectal cancer; RC, rectal cancer.

weight loss (online supplemental figure 2A), suggesting that C3aR protects from excessive intestinal inflammation. This result agrees with previous literature showing that lack of complement activation in *C3*^{-/-} mice exacerbates chronic intestinal inflammation.³³ Notably, as shown in online supplemental figure 2B-D, *C3aR*^{-/-} mice developed significantly higher tumor numbers and higher tumor load in the colon than the WT mice, with a predominance of larger tumors (>2 mm). As innate and adaptive immune responses are involved in colon inflammation and tumorigenesis, we set up three interlinked flow cytometry panels to characterize the immune infiltrates in the colon adenocarcinoma generated following AOM/DSS treatment and the mesenteric lymph nodes (mLNs). As shown in online supplemental figure 2E-G, we found higher numbers of CD11c⁺ macrophages in the mLN of *C3aR*^{-/-} mice than WT, with no significant

differences in the other cell populations. In the tumors, in addition to higher numbers of CD11c⁺ macrophages (online supplemental figure 2H), in the *C3aR*^{-/-} mice, we detected significantly enhanced levels of activated CD4⁺ T cells (CD4⁺CD25⁺ FoxP3⁺) and interferon gamma (IFN- γ)⁺ CD4⁺ (Th1) (online supplemental figure 2I,J) compared with WT mice.

Although more than 20% of individuals with IBD develop CRC, intestinal inflammation accounts for only about 2% of total CRC.³⁴ Therefore, we next investigated the impact of C3aR loss in the APC^{Min/+} spontaneous model, which, like 80% of human CRC, carries a mutation of the *apc* gene.³⁵ We generated APC^{Min/+} mice lacking the *c3ar1* gene (APC^{Min/+}/*C3aR*^{-/-}) and compared tumor development in the colon from 5 weeks to 28 weeks of age APC^{Min/+} and APC^{Min/+}/*C3aR*^{-/-} mice. We and others have shown that in APC^{Min/+} mice, CRC

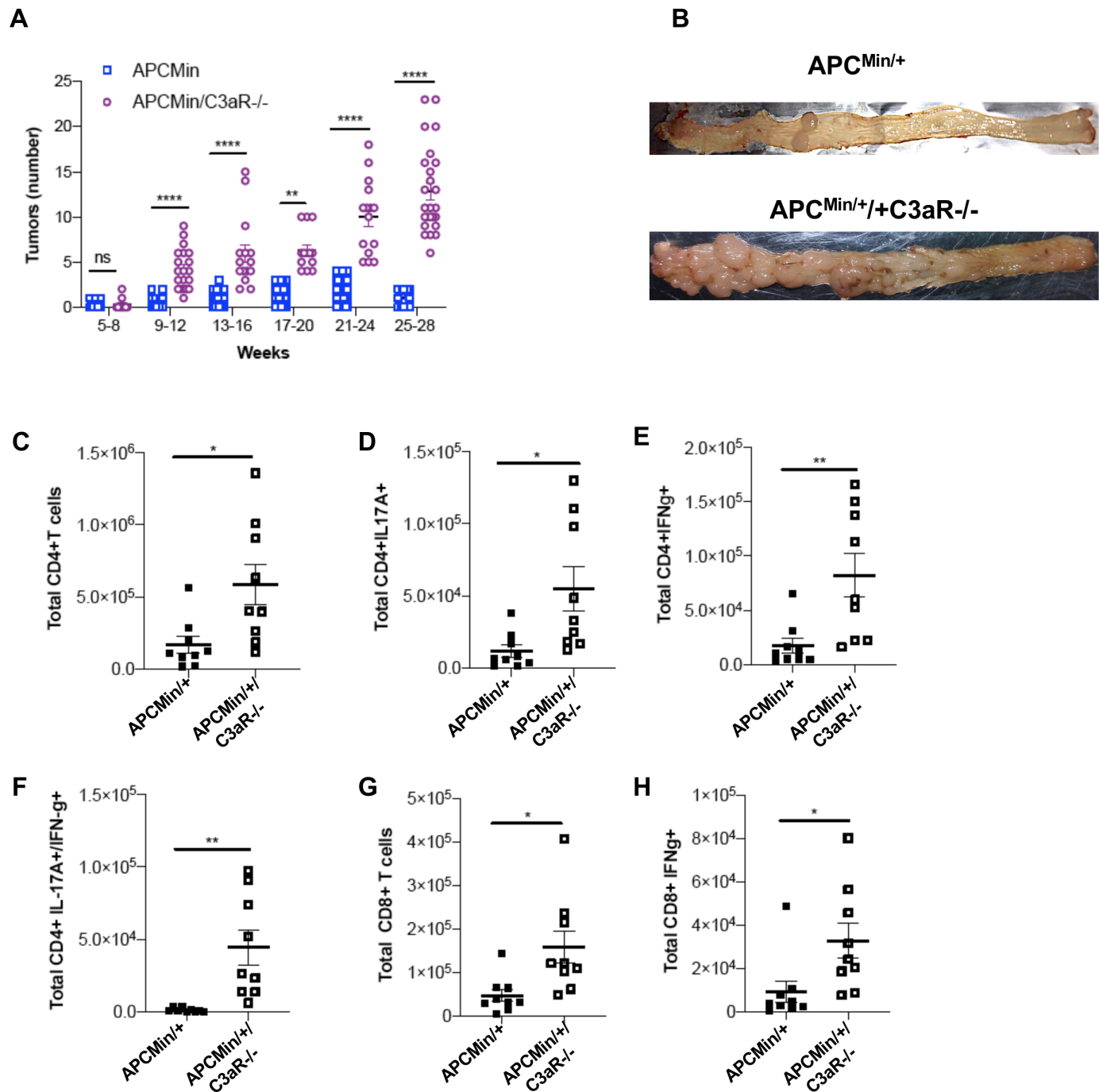


Figure 2 Loss of C3aR switches tumorigenesis from small intestine to colon in APC^{Min/+} mice and promotes increased immune cell infiltration. (A) Tumor numbers in the colon of APC^{Min/+} and APC^{Min/+}/C3aR^{-/-} from weeks 5 to 28 weeks of age. (B) Representative picture of tumor number and distribution in the colon of APC^{Min/+} and APC^{Min/+}/C3aR^{-/-} mice. Single-cell suspensions from cLP of APC^{Min/+} and APC^{Min/+}/C3aR^{-/-} mice were analyzed by flow cytometry. Shown are the total number of (C) CD4+ T cells, (D) Th17 cells, (E) Th1 cells, (F) Th1/Th17 cells, (G) CD8+ T cells, and (H) Tc cells (CD3+CD8+IFN-γ+). A significance was calculated using two-way analysis of variance with Bonferroni post-test and a minimum of 10 mice/group. In panels, (C–H) Results are pooled from two independent experiments with a minimum of nine mice/group. Significance was calculated using unpaired t-test. *P<0.05, **P<0.01, ****P<0.0001. C3aR, C3a receptor; cLP, colon lamina propria; IFN-γ, interferon gamma; IL, interleukin; ns, not significant.

development is seldom, with the highest tumor burden in the small intestine.^{13 36} In line with the human data and the results in the model of inflammation-driven CRC, we found that in the absence of C3aR, starting at 10 weeks of age, APC^{Min/+} mice showed a shift of tumorigenesis

from the small intestine to the colon with the highest localization in distal colon and rectum (figure 2A,B). Similar to the approach used in the AOM/DSS model, we performed flow cytometry to quantify the immune infiltrate associated with tumor development. Due to the

insufficient number of colon tumors in APC^{Min/+} mice, we analyzed the mLN and the cLP. In agreement with our findings in the AOM/DSS model, loss of C3aR resulted in significantly higher numbers of Th17, Th1, Th1/Th17, and CD8+ T cells in the cLP of APC^{Min/+}/C3aR^{-/-} mice compared with the APC^{Min/+} counterpart (figure 2C–H). In the mLN, we found higher numbers of CD4+ and CD8+ T cells in the APC^{Min/+}/C3aR^{-/-} mice compared with APC^{Min/+} mice, but functional differences were only limited to higher numbers of IFN- γ -producing CD8+ T cells in APC^{Min/+}/C3aR^{-/-} mice (online supplemental figure 3A–F). Altogether, these results demonstrate that loss of C3aR unleashes a colon-specific inflammatory program.

Loss of C3aR results in altered gut microbiota that supports tumor growth in the colon of APC^{Min/+} mice

Several evidences suggest that the microbial flora strictly influences CRC development and immune signature.^{37–39} Therefore, to assess the functional role of the microbiota in tumor development in our model, we first set up to understand whether the transfer of APC^{Min/+}/C3aR^{-/-} microbiota could induce tumor development in the colon of APC^{Min/+} mice. To this aim, tumor-free, 5-week-old APC^{Min/+} mice were treated with broad-spectrum antibiotics, then administered via gavage with fecal and tumor-associated microbiota from 12-week-old APC^{Min/+}/C3aR^{-/-} mice or APC^{Min/+} mice and sacrificed at the age of 12 weeks (figure 3A). As shown in figure 3B, while APC^{Min/+} mice receiving the APC^{Min/+} microbiota developed very few tumors in the colon, the transfer of the APC^{Min/+}/C3aR^{-/-} microbiota resulted in increased tumor burden in the colon, with no changes in the total number of small intestinal tumors (online supplemental figure 4A,B). To test whether the microbiota could also affect the phenotype and functions of the immune cells in the colon of microbiota-transplanted mice as observed in the donors, we characterized the immune cell infiltrates in APC^{Min/+} mice receiving APC^{Min/+} or APC^{Min/+}/C3aR^{-/-} microbiota. As shown in figure 3C–H and online supplemental figure 4C–H, APC^{Min/+} mice receiving APC^{Min/+}/C3aR^{-/-} microbiota showed higher tumor numbers in the colon and increased Th1, Th17, and Th1/Th17 cells as well as IFN- γ -producing CD8+ T cells.

Next, to understand whether the results obtained with the microbiota transplantation were the consequence of a tumor-induced microbiota or a change in microbiota composition driven by C3aR deficiency, we characterized the microbiota before and after tumor development. For this purpose, we collected the fecal pellets from tumor-free (8-week-old) and tumor-bearing (12-week-old) APC^{Min/+} and APC^{Min/+}/C3aR^{-/-} mice. Feces from age-matched and sex-matched WT and C3aR^{-/-} were used as controls. The V5–V6 hypervariable regions of bacterial 16S rRNA genes in feces were amplified, and the obtained libraries were sequenced on the MiSeq Illumina platform. Compared with controls, we observed higher alpha diversity in 8-week-old APC^{Min/+}/C3aR^{-/-} and C3aR^{-/-} mice

measured by observed ASV, Faith, and Shannon indices (figure 4A). The alpha diversity was normalized in 12-week-old mice, although there was still a clear separation among the two mouse strains in terms of beta diversity (figure 4B). These results support the concept that the fecal microbiota that precedes tumor growth is highly diversified within the same group.

In contrast, the selection of defined bacterial species reduced intragroup and enhanced intergroup diversification on tumor development. When examining the most abundant phyla differences, we observed that already at 8 weeks, when the mice in our colony are devoid of tumors in both small intestine and colon, in APC^{Min/+}/C3aR^{-/-} mice, there was an increase in Bacteroidetes and Proteobacteria. Further, there was an evident reduction of Firmicutes compared with APC^{Min/+} mice. These differences became even more striking at 12 weeks when we could see the first differences in colon tumorigenesis (figure 4C). Notably, Bacteroidetes are significantly upregulated in the stool-associated microbiota of patients with CRC and have been correlated with elevated Th17 in their tumor-adjacent mucosa.^{40–41} To determine whether the differences found in the fecal microbiota were mirrored at the tumor site, we additionally sequenced the mucus-associated and tumor-associated bacteria in 12-week-old APC^{Min/+} and APC^{Min/+}/C3aR^{-/-} mice. As shown in online supplemental figure 5A,B, despite the bacterial composition in tumor and mucus of the two mouse strains being more similar than that in the stool and was dominated by Firmicutes, the tumor-associated microbiota in APC^{Min/+}/C3aR^{-/-} mice still showed a higher abundance of Bacteroidetes. These results closely mirror the bacterial composition in CRC, where Firmicutes is the predominant phylum in the cancerous tissues, followed by Bacteroidetes.⁴²

Altogether, these results suggest that lack of C3aR promotes the establishment of a fecal microbiota that is among the drivers of tumor development and proinflammatory immune responses.

Loss of C3aR converts cold tumors into hot tumors

To more thoroughly determine how the lack of C3aR shapes the TME and the adjacent mucosa in our model of spontaneous colon tumorigenesis, we performed RNA-Seq analysis. First, we compared the transcriptomic profile of colon tumors developed by 12-week-old APC^{Min/+} and APC^{Min/+}/C3aR^{-/-} mice. We found 72 downregulated genes and 369 upregulated genes in colon tumors from APC^{Min/+}/C3aR^{-/-} mice, clearly indicating that loss of C3aR affects the transcriptomic profile of the polyps (figure 5A,B).

Notably, iPathway analysis revealed that the top 25 Gene Ontology (GO) biological processes associated with differentially expressed genes in the polyps were related to innate and adaptive immune responses (figure 5C). Accordingly, using the edgeR-GLM framework (see Materials and methods), we found significant upregulation of genes associated with defense response. These genes were

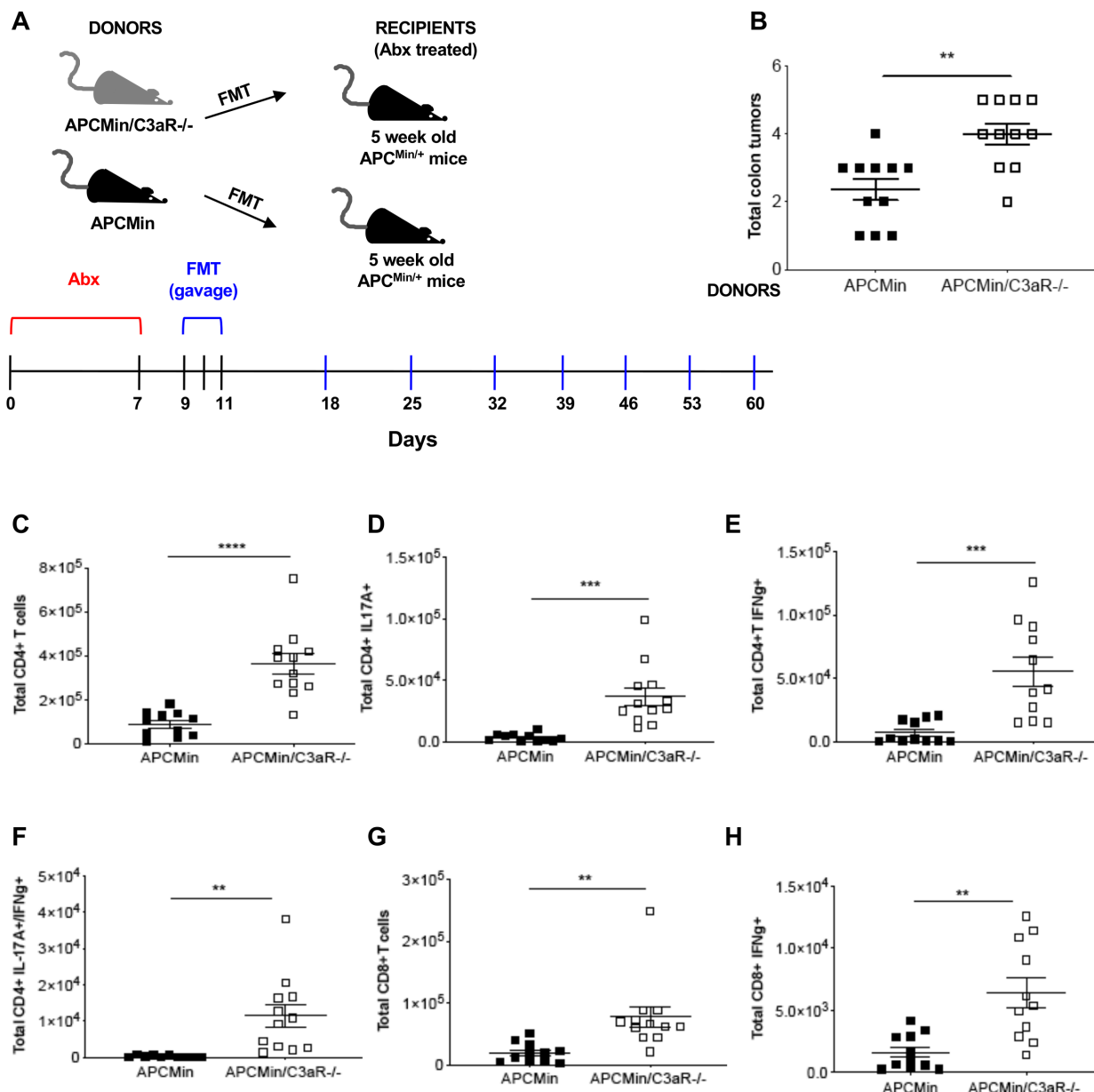


Figure 3 Transplantation of the APC^{Min/+}/C3aR^{-/-} microbiota transfers inflammation and colon tumorigenesis to APC^{Min/+} mice. (A) Treatment scheme for 5-week-old APC^{Min/+} mice (recipients) transplanted with the microbiota of 12-week-old APC^{Min/+} or APC^{Min/+}/C3aR^{-/-} mice (donors). (B) Tumor counts in the colon of recipient mice. (C–H) Flow cytometry analysis of cLP infiltrating lymphocytes showing total cell number of (C) CD4⁺ T cells, (D) Th17 cells, (E) Th1 cells, (F) Th1/17 cells, (G) CD8⁺ T cells, and (H) cytotoxic T (Tc) cells. Shown are the results of two independent experiments with 11 mice/group. Significance was calculated using unpaired t-test. **P<0.01, ***P<0.001, ****P<0.0001. C3aR, C3a receptor; cLP, colon lamina propria; FMT, fecal microbiota transplantation; IFN-γ, interferon gamma; IL, interleukin

cd8, *ccr6*, *il21*, *cd19*, and *il22ra2*; IFN-γ-mediated signaling pathway-related genes, such as *if* and guanylate-binding protein family genes *tap-1*, *ciita*, *b2-microglobulin*, and *stat1*; genes associated with development and maturation of innate immune cells and response to type I interferon such as *irf4* and *irf8* and *cd83*; negative regulators of the immune response, such as *btlA*, *cd274* (*pd-1*), *cd40lg*, and *ido1*; genes associated with leukocyte migration such as *cxcl9*, *cxcl10*, *cxcl11*, and *cxcr5*; and NK cell activation genes such as *il-12b* and *ncr1*. Among the significantly downregulated genes, we found genes for transporters including *slc47* and *slc44a5* and Wnt signaling pathway inhibitors

such as *dkk2* and *dkk3* (figure 5D). The latter mediates the failure of anti-PD-1 treatment in patients with MSS-high CRC by dampening NK and CD8-mediated antitumor immune responses.⁴³

Similar to the approach used for the TME, we performed RNA-Seq analysis on the distal colon of the same APC^{Min/+} mice and APC^{Min/+}/C3aR^{-/-} using WT and C3aR^{-/-} as respective controls. The comparison revealed that APC^{Min/+} mice had a transcriptomic profile closer to WT mice than to APC^{Min/+}/C3aR^{-/-} mice, and similarly, healthy colons of C3aR^{-/-} mice exhibited a transcriptomic profile more similar to the colons of APC^{Min/+}/

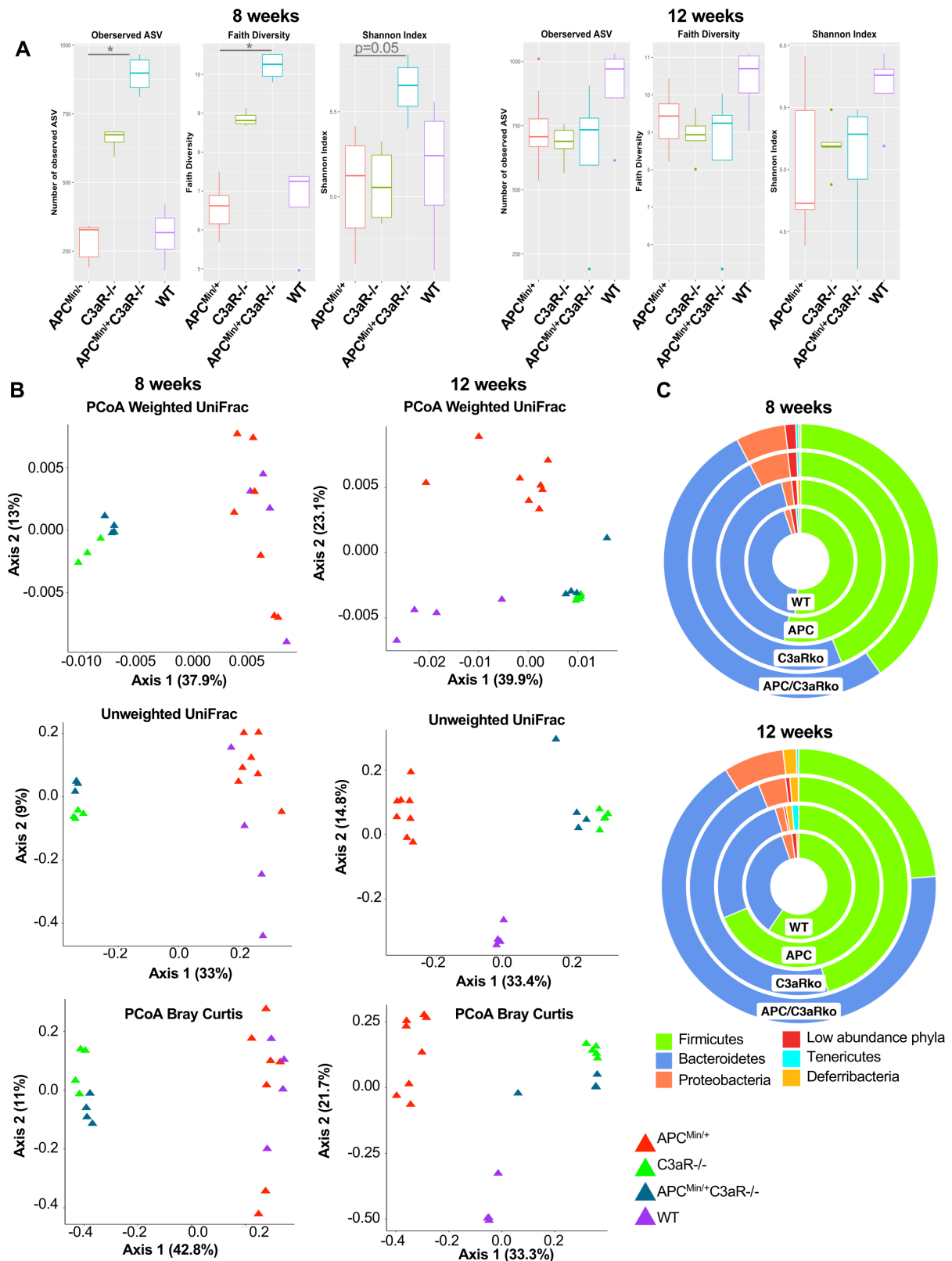


Figure 4 Loss of C3aR affects the composition of the fecal microbiota in APC^{Min/+} mice. Bacterial DNA was extracted from the feces of 8- and 12-week-old APC^{Min/+}, APC^{Min/+}/C3aR^{-/-}, C3aR^{-/-} and WT mice, and bacterial profiling was performed by sequencing the V5-V6 hypervariable of 16S rDNA using Illumina MiSeq platform. (A) Plots showing alpha diversity evaluated by observed ASV, Faith, and Shannon Index in 8- and 12-week-old mice. (B) Principal Coordinates Analysis (PCoA) showing the beta diversity assessed by the three inferred Beta Diversity metrics (weighted UniFrac, unweighted UniFrac, and Bray-Curtis) in mice 8 and 12 weeks old. (C) Doughnut charts showing phylum abundance at 8 and 12 weeks. Four to eight mice/group were used. Significance was calculated using (A) the Kruskal-Wallis test, followed by a pairwise Wilcoxon as post-test; (B) PERmutational Multivariate ANOVA (PERMANOVA) test; and (C) DESeq R-package. C3aR, C3a receptor.

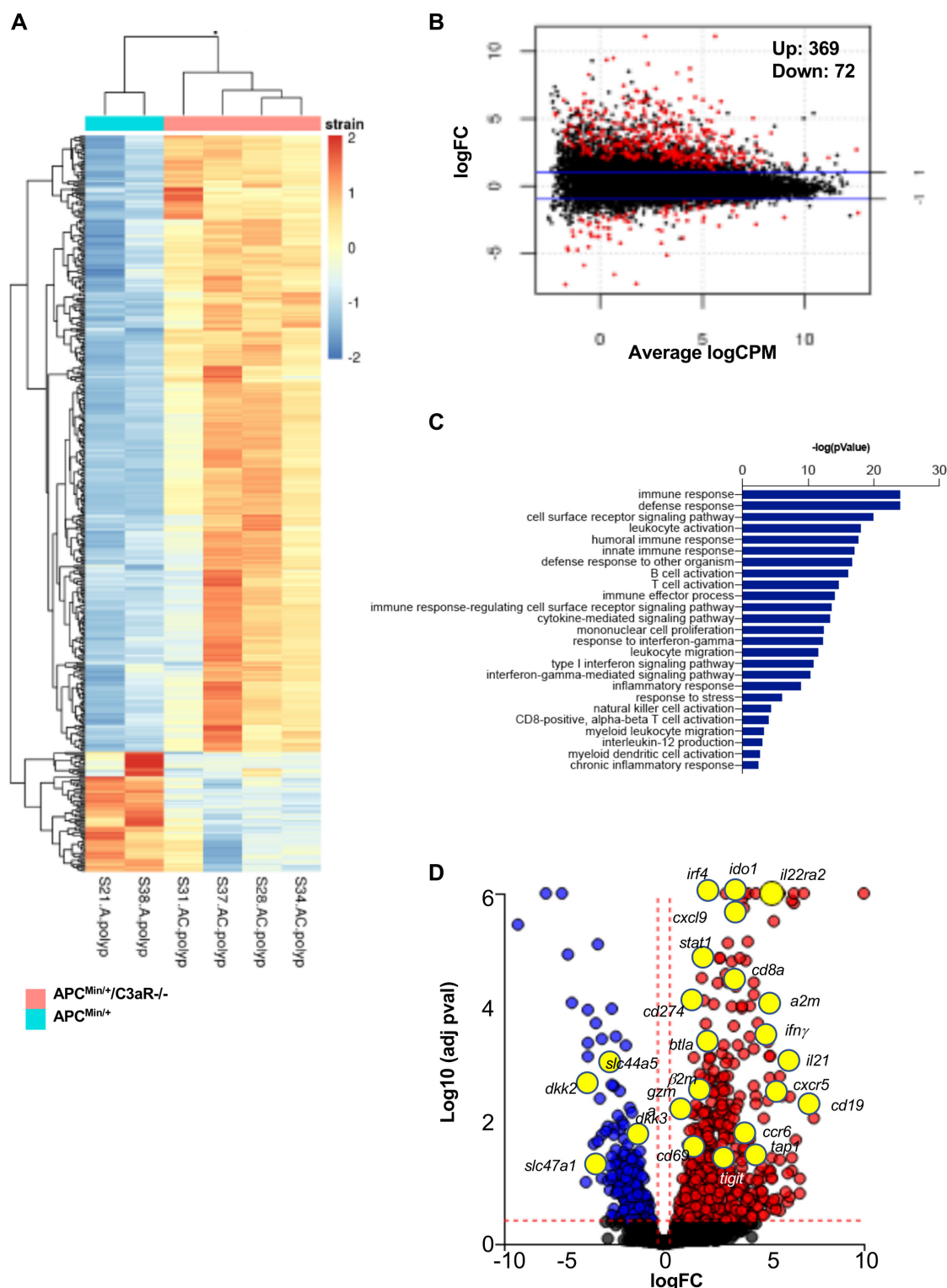


Figure 5 Tumors in APC^{Min/+}/C3aR^{-/-} show enrichment in innate and adaptive inflammatory pathways. (A) Heatmap from log counts per million values using data from colon polyps from APC^{Min/+} and APC^{Min/+}/C3aR^{-/-} mice. (B) Summary plot showing the number of significant differentially expressed genes in polyps of APC^{Min/+} and APC^{Min/+}/C3aR^{-/-} mice. The plot displays log fold change against log counts per million for each gene. The red points represent significant differentially expressed genes, and the horizontal blue lines indicate a twofold increase or decrease in expression. (C) Visualization of the gene-associated GO biological processes in the polyps. (D) Volcano plot showing the fold change magnitude for all genes differentially expressed in the polyps of APC^{Min/+}/C3aR^{-/-} versus APC^{Min/+} mice (n=4). Significantly upregulated and downregulated genes belonging to the GO biological processes (B) are highlighted in yellow. Vertical and horizontal red dotted lines indicate the threshold. Significance was calculated using the edgeR function `decideTestsDGE` with Benjamini-Hochberg correction for FDR; a default FDR threshold of 0.05 and a log₂ fold change threshold of 0.6 were applied. C3aR, C3a receptor; FDR, false discovery rate; GO, Gene Ontology.

C3aR^{-/-} than to the colons of WT mice (online supplemental figures 6A–F and 7A). Notably, iPathway analysis revealed that the top 25 GO biological processes associated with differentially expressed genes were related to innate and adaptive immune responses (online supplemental figure 7B,C).

Since tumor development in APC^{Min/+} mice is driven by Wnt signaling, which results in immune exclusion and MSS-like phenotype, our findings indicate that the loss of C3aR is sufficient to promote a vigorous immune signature in the colon and the tumors of APC^{Min/+} mice, therefore converting cold tumors into hot tumors.

C3aR expression in patients with cancer affects the infiltration of innate and adaptive immune cells

Our C3aR expression data in the patients with colon and rectal cancers and our mouse model prompted us to search the CBIOportal database for how C3aR expression affects the immune contexture in the human TME. We obtained the RNA expression for *c3ar1* and immune cell signatures from 231 cases of rectal cancer and 97 cases of colon cancer in the FOxTROT cohort (https://ascopubs.org/doi/abs/10.1200/JCO.2019.37.15_suppl.3504) using CIBERSORT, xCell and MCP (online supplemental table 1).^{44–47} Cell populations showing significant positive or negative correlation with C3aR with two out of three methods in both patients with rectal and colon cancers are reported in figure 6. Pearson and Spearman correlation analyses revealed that in patients with rectal and colon cancers reduced expression of *C3ar1* resulted in an increased level of innate and adaptive immune cells, which have been associated with better response to anti-PD1 immunotherapy in several solid malignancies, including CRC, such as activated NK, CD8+ T, B cells, memory CD4+ T cells and Tregs^{5 45 46} (figure 6A,C). Conversely, our analysis revealed that higher expression of *C3ar1* positively correlated with several immune cells that can contribute to the generation of an immunosuppressive TME or can directly inhibit cytotoxic immune responses by inducing tolerance such as resting NK cells, macrophages, neutrophils, and resting dendritic cells (DCs) (figure 6B,D).^{48 49} Therefore, confirming our earlier results in our novel mouse model, results showed that the C3aR status may have substantial implications for treating patients with colon and rectal cancers with immunotherapy using ICB.

Lack of C3aR confers susceptibility to treatment with anti-PD-1

Based on the results on the human dataset and the findings in our mouse model showing an increased innate and adaptive immune response and the expression of checkpoint blockade molecules such as PD-L1 and an IFN signature, we next investigated whether this signature confers response to ICB therapy in APC^{Min/+}/C3aR^{-/-} mice. To perform a treatment regimen that would more closely resemble the clinical setting, APC^{Min/+}/C3aR^{-/-} mice were treated with a-PD-1 or with the control antibody twice a week for 5 weeks starting at the age of 12 weeks when colon tumors are already established in our colony. As shown in figure 7A, at

sacrifice, we found that relative to their untreated controls, the vast majority of APC^{Min/+}/C3aR^{-/-} mice treated with a-PD-1 showed a significant reduction in tumor number and load, which demonstrates that a-PD-1 is not only effective at reducing the development of new tumors but also can significantly reduce the size of already established tumors. After ICB treatment, mass cytometry was used to determine tumor-infiltrating immune cells' overall composition and function. To this aim, we developed and validated a mass cytometry panel encompassing markers to define cell types and a set of cytokines to define immune cell functions, which were analyzed following our previously published bimatrix analysis (table 1 and online supplemental figure 8).⁵⁰

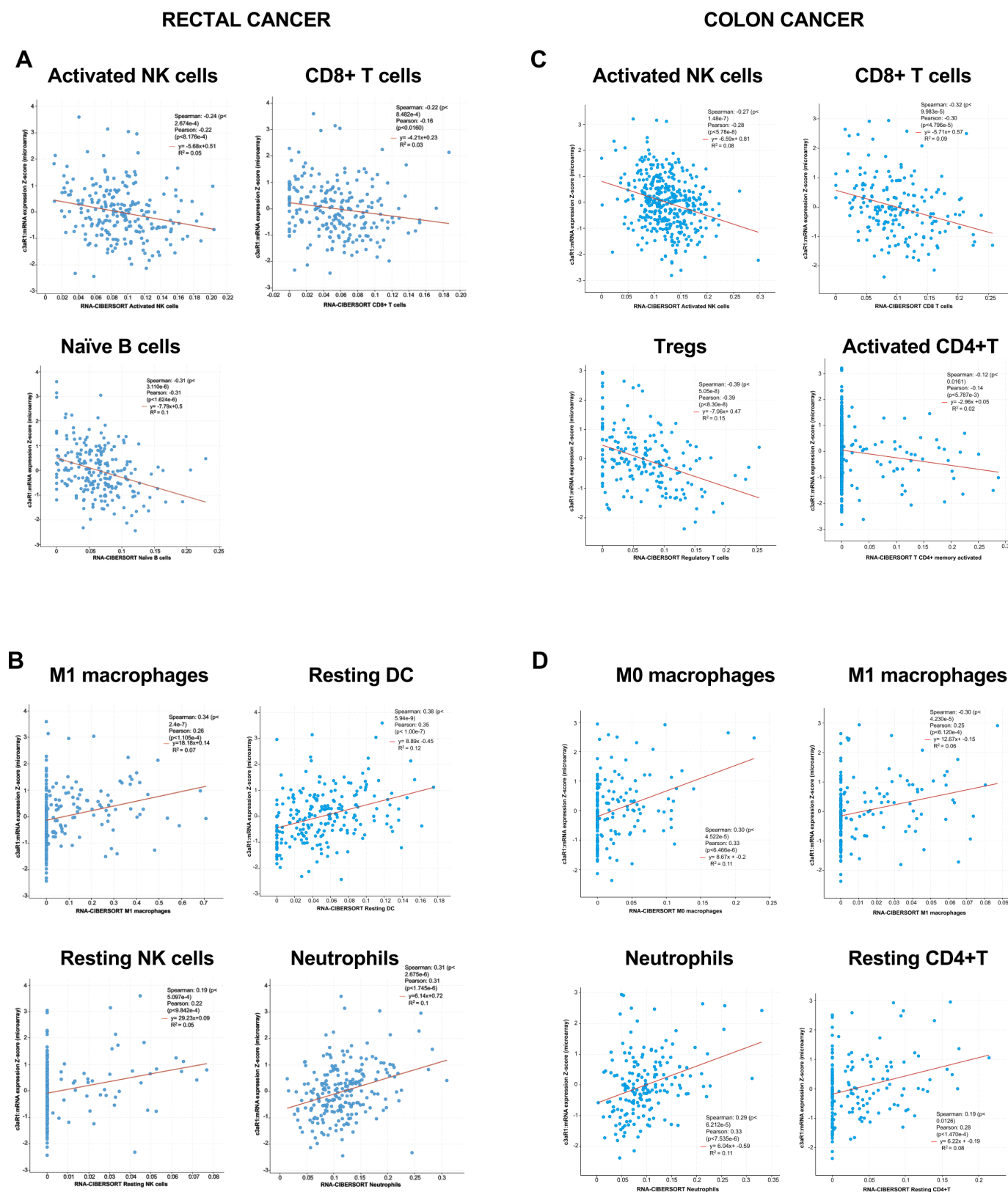
Briefly, after annotating immune cell types using only the type markers (figure 7B), we considered an entire cytokine set profile for each cell type. The cells were then clustered using the self-organizing map (SOM) method in 10 times 10 grid to generate a profile of potential 100 cytokine-producing clusters per cell type. Following a-PD-1 treatment, we found increased frequencies of intratumoral polyfunctional NK cells expressing interleukin (IL)-2, IL-12, and IFN- γ and downregulation of an NK cluster expressing IL-6, IL-4, and IL-22. In addition, although our mass cytometry panel was not designed to study ILC specifically, we also found a parallel reduction of an anti-inflammatory ILC-like cell cluster producing IL-4 and IL-22 (figure 7C). These results agree with a recent study in human CRC, which described in the tumor tissues of MSI-H CRC an innate immune signature characterized by increased levels of cytotoxic innate lymphoid cells and NK cells.⁵¹ Furthermore, we found increased frequencies of DC, macrophage, and monocyte clusters expressing IL-6 and tumor necrosis factor alpha (TNF- α). Notably, six out of seven significantly downregulated lymphoid and myeloid cell clusters expressed IL-22. Further, TNF- α and IL-12 producing Nkp22, a cell type that has been shown to support CRC development, were downregulated following a-PD-1 therapy.

Overall, our results show that the inflammatory signature in APC^{Min/+}/C3aR^{-/-} tumors confer susceptibility to ICB therapy.

DISCUSSION

Inflammation in CRC plays a paradoxical role. For instance, inflammatory immune responses fuel tumor development and progression, and the use of anti-inflammatory agents lowers sporadic CRC-related mortality.⁵² Conversely, the presence of an inflammatory immune infiltrate is essential to promote antitumor immunity and correlates with increased survival in patients with CRC.⁸ This evidence suggests that there may be options to exploit the underlying mechanisms of cancer-promoting inflammation to treat the disease more efficiently.

We describe the downregulation of the receptor for the complement anaphylatoxin C3a (*C3ar1*) in subsets of patients with CRC. Furthermore, we found that reduced C3aR expression in patients with cancer correlates with



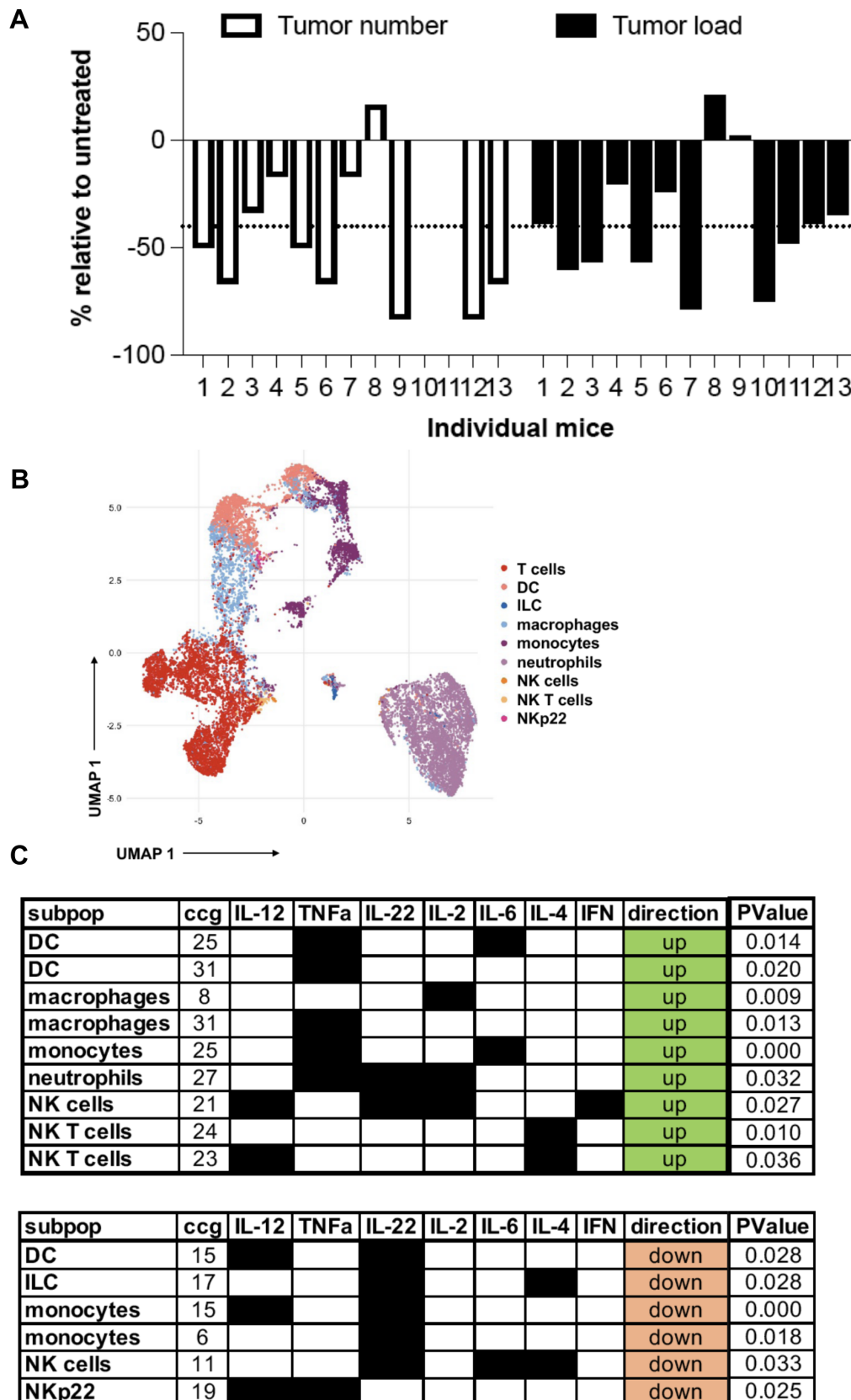


Figure 7 Lack of C3aR confers susceptibility to treatment with a-PD-1 treatment. (A) Tumor number and load in individual APC^{Min/+}/C3aR^{-/-} mice treated for 5 weeks with a-PD1 expressed as % reduction over the mice treated with the control antibody. (B) Visualization of 70 000 pooled events from a-PD1 and control mice using the uMAP algorithm. (C) The functional profile of cell clusters that were significantly upregulated or downregulated in anti-PD1-treated mice compared with control was visualized by using the bimatrix approach. The results of two independent experiments with a minimum of 11 mice/group are shown. DC, dendritic cell; IFN, interferon; IL, interleukin; ILC, innate lymphoid cells; NK, natural killer.

increased numbers of innate and adaptive antitumor immune cells in the TME. Reverse-translation in vivo uncovered that loss of C3aR enhances tumor development in a model of inflammation-driven CRC. Additionally, loss of C3aR was sufficient to induce colon tumorigenesis in the spontaneous APC^{Min/+} model, which usually shows a prevalence of tumors in the small intestine and seldom colon tumors. As such, our novel mouse of colon carcinogenesis represents an important contribution to the field where progress toward chemoprevention and treatment has been largely hindered by the sparsity of reliable models to closely mirror the human disease. Specifically, the generation of the APC^{Min/+} mouse following mutagenesis screening historically enabled the critical discovery of the central role of *apc* inactivation for the development of CRC.^{53 54} However, the development of multiple tumors in the small intestine rather than in the colon of APC^{Min/+} mice does not only poorly recapitulate the anatomical location of the human disease but also carries several additional shortcomings. Relevant publications in the field of CRC have tried to recapitulate the human disease by developing APC-based models of colorectal tumorigenesis such as the CPC-APC mice obtained by crossing the APC^{fllox/wt} with the CDX2-cre, which targets APC inactivation to the colon, therefore resulting in the development of adenomas in the distal colon.⁵⁵ More recent data have also shown that the treatment with the carcinogen AOM can induce the development of tumors also in absence of the cre recombinase, but the underlying mechanism is poorly understood.⁵⁶ Although the use of the cre-lox system deserves cautions and can have many pitfalls,⁵⁷ it would be highly relevant to assess how the loss of C3aR in the CPC-APC system affects the number and the immune infiltration of colon tumors. In the herein described model by knocking out the receptor for the complement anaphylatoxin C3a (C3aR) in the APC^{Min/+} mice, we were not only able to achieve the development of several polyps in the colon but were also able to achieve a drastic reduction of tumors in the small intestine¹³ (online supplemental figure 9). As result, APC^{Min/+}/C3aR^{-/-} mice are devoid of several shortcomings that we and others have described in the APC^{Min/+} model such as ulcerations of the gastrointestinal tract that cause progressive increase in blood loss, development of hypercoagulation, anemia and splenomegaly and have a longer lifespan compared with APC^{Min/+} mice.¹³

Furthermore, similar to the findings in patients, the tumors developing in the absence of C3aR showed enhanced infiltration by innate and adaptive immune cells. This signature depended on the fecal and tumor-associated microbiota, and we provided evidence that this tumor-associated immune cell signature can be exploited for ICB therapy.

Several mechanisms could potentially mediate C3aR downregulation or inactivation in human CRC. In this context, it is essential to note that, while genetic mutations in the complement system as a group occur at a significantly higher rate than in any other gene for several

cancers, most individual complement genes mutate at a lower rate than many canonical oncogenes and oncosuppressors.²⁹ Accordingly, we found that in patients with CRC compared with healthy controls, there is a significantly higher frequency of C3aR methylation occurring in those regions likely to result in mRNA expression changes.

One of the most striking findings in our study is that lack of C3aR resulted in significant upregulation of immune signatures in the tumors and adjacent mucosa. Specifically, we found increased Tregs, Th17 and Th1/Th17, and IFN- γ -producing CD8 T cells. The role of IL-17 in CRC is highly debated. Data in patients and mouse models of CRC showed that IL-17 production by different cell sources promotes the inflammatory process and fosters cancer cell proliferation.^{58 59} On the other hand, the production of IL-17A is essential to preserve the integrity of the epithelial barrier, and published literature showed that Th17 in human CRC could recruit CD8+ T cells.⁶⁰ The higher abundance of Th17 cells could be directly linked to the increased levels of *il-21* in APC^{Min/+}/C3aR^{-/-} compared with APC^{Min/+} mice as shown by our RNA-Seq data. There is abundant evidence in the literature showing that IL-21 plays a crucial role in the differentiation of Th17 cells.^{61 62} Interestingly, the data on the effect of IL-21 in antitumor immunity and CRC development are somewhat conflicting. Specifically, in several preclinical models, IL-21 has been shown to potentiate antitumor immunity by supporting the cytotoxic activity of CD8+ T and NK cells, the proliferation of Th1 and Th17 cells and the antigen presentation by DCs.⁶³ As such, it has undergone phase I and II clinical trials for several cancers with overall promising results.^{64–66} However, in the context of CRC, while one study in APC^{Min/+} mice confirmed the antitumorigenic role of IL-21,⁶⁷ other studies have shown that both in sporadic and inflammation-driven CRC, IL-21 supports CRC development.^{68–70} These findings were confirmed in patients with CRC by De Simone *et al*, who additionally showed that IL-21 upregulation in the tumors of patients with CRC is mostly driven by the infiltrating CD8+ T cells.⁷¹

In addition, lack of C3aR also resulted in upregulation of innate immune signatures suggestive of enhanced antigen presentation. Overall, these findings are surprising because *apc* mutations result in Wnt-driven tumors that have an MSS phenotype, with the exclusion of immune cells from the TME and consequent resistance to ICB therapy.⁷²

The finding that immune responses can both promote the tumor development and be exploited to increase the efficacy of current anticancer treatments was also emphasized in a recently described dual oncogene mouse model of CRC. In this model, DeStefano Shields and collaborators showed that the administration of the enterotoxigenic *Bacteroides fragilis* promoted the development of colon tumors in mice carrying both the APC^{Min/+} (Min^{Ap Δ 716/+}) and the human BRAF^{V600E} mutations.⁷³ Interestingly, in these mice, the increased tumorigenesis

was accompanied by a Th1 signature in the TME with increased CD8⁺ T cells and expression of checkpoint inhibition molecules, which rendered the tumor responsive to anti-PD-L1 treatment.

The mechanistic reasons underlying these opposing roles of the immune system in cancer are the object of active investigations in the field. Two recent reports suggested that cancer cells can exploit even transient inflammatory conditions to undergo epigenetic reprogramming, and once they established the tumor, they exploit the selective pressure of the immune system to develop genetic alterations that enable their immune evasion.^{74,75}

Our finding that MSS colon tumors lacking C3aR are responsive to anti-PD-1 treatment indicates that the identified immune signature has a positive prognostic value and that C3aR may serve as an additional checkpoint in ICB therapy of CRC. Previous studies have shown that inhibition of the complement anaphylatoxin C5aR enhances ICB response in immunologically hot tumors, such as lung cancer and melanoma.^{76,77} Based on our findings, we propose that dysregulation of the C3a–C3aR axis in CRC renders ‘cold’ tumors ‘hot’ rather than simply deblocking infiltrating immune cells. Notably, while we found that almost all animals responded to a-PD-1 therapy, with half of them achieving over 50% reduction in tumor number and tumor load, we also observed a lack of response in a few cases. These results are compatible with the ICB treatment in human CRC, where a-PD1 alone confers an overall response rate of 31% in patients with MSI-H CRC, which can be increased to 55% by the combination with a-CTLA-4.⁸

While CD4 and CD8 T cells are the main targets of anti-PD-1 therapy, checkpoint therapies’ efficacy depends on innate immunity.⁷⁸ Specifically, increased frequencies of DC, monocytes, and macrophages producing TNF- α and IL-6 on treatment with anti-PD-1 indicate a direct effect of ICB on these myeloid cells. This is supported by published data showing that PD-1-expressing macrophages have a protumorigenic phenotype and that a-PD-1 therapy reverses this trend, increasing the expression of TNF- α , iNOS, and IL-6, which potentiate antitumor immunity.⁷⁹ Additionally, we found that among the most downregulated cytokines in innate lymphoid and myeloid cell clusters, there was IL-22, which can support CRC growth by directly acting on epithelial cells.⁸⁰ This finding is particularly interesting in light of our RNA-Seq data showing significantly higher expression of *il-22ra2* in the polyps of APC^{Min/+}/C3aR^{-/-} mice compared with APC^{Min/+} mice. IL-22RA2 is also known as IL-22 binding protein (IL-22BP) and limits IL-22 bioavailability by preventing its binding to the IL-22- α 1. Seminal work in the field has shown that IL-22RA2^{-/-} mice develop more colon tumors as a result of an enhanced IL-22-driven epithelial cell proliferation.⁸¹ DCs have been initially described as the main cells expressing IL-22ra2. However, Pelczar and collaborators unraveled a pathogenic role for the IL-22RA2 produced by CD4⁺ T cells, therefore suggesting that the

cellular source of IL-22RA2 may be relevant for its function.⁸² Accordingly, based on our finding that the tumors from APC^{Min/+}/C3aR^{-/-} mice are highly infiltrated by T cells, it is likely that the IL-22RA2-producing CD4⁺ T cells fuel the pre-existing inflammation associated with the protumorigenic microbiota ultimately supporting tumor growth. It remains to be determined whether, similar to the anti-TNF- α treatment, a-PD1 therapy can selectively affect the expression of IL-22RA2 in CD4⁺ T cells.

A caveat of our finding on *il-22ra2* is that the increased RNA levels may not necessarily correlate with the protein levels.

Our study also unraveled that the fecal microbiota of APC^{Min/+}/C3aR^{-/-} and C3aR^{-/-} mice carried a higher abundance of Gram-negative bacteria such as Bacteroidetes and Proteobacteria. Based on the results of our FMT experiments, the fecal microbiota established in the absence of C3aR is likely the main driver of tumor development and the immune infiltrate in the colon of APC^{Min/+} mice. Conversely, the similarity between APC^{Min/+} and APC^{Min/+}/C3aR^{-/-} mice may suggest that the physiological and metabolic alterations occurring in the TME represent the main constraint that dictates the specific composition of the microbial community. The similarity in the overall composition does not exclude the blooming in the TME of APC^{Min/+}/C3aR^{-/-} of more pathogenic bacterial strains that can further support tumor growth and therefore play a more pronounced role at the later stages in agreement with the driver-passenger theory.⁸³ However, considering the significant differences described in the fecal microbiota of patients with CRC and healthy controls, it is tempting to speculate that in the clinical setting, the composition of the indigenous rather than the tumor-associated microbiota may be a more relevant indicator for the risk of developing CRC.

Altogether, we reported here for the first time that the complement C3a–C3aR axis represents the Achilles’ heel of CRC. The complement system in the gastrointestinal tract is essential to avoid overt inflammation in health conditions. However, this regulatory mechanism may restrain the activation of immune responses during tumor development. Thus, the C3a–C3aR axis can be a previously unrecognized checkpoint to enhance anti-tumor immunity in CRC.

Author affiliations

¹Department of Pathology and Laboratory Medicine, Medical University of South Carolina, Charleston, South Carolina, USA

²Hollings Cancer Center Charleston, Medical University of South Carolina, Charleston, South Carolina, USA

³Institute of Molecular Life Sciences, University of Zurich, Zurich, Switzerland

⁴SIB Swiss Institute of Bioinformatics, University of Zurich, Zurich, Switzerland

⁵Institute of Biomembranes, Bioenergetics and Molecular Biotechnologies, Consiglio Nazionale delle Ricerche, Bari, Italy

⁶School of Biological Sciences and Institute for Global Food Security, Queens University of Belfast, Belfast, UK

⁷Institute of Radiation Oncology, Medical Research Council Oxford Institute for Radiation Oncology, Oxford, UK

⁸Host-microbe Metabolic Interactions, Microbiology, University of Groningen, Groningen, The Netherlands

⁹Department of Microbiology and Immunology, Medical University of South Carolina, Charleston, South Carolina, USA

¹⁰Regenerative Medicine and Cell Biology, Medical University of South Carolina, Charleston, South Carolina, USA

¹¹Department of Experimental Oncology, IEO European Institute of Oncology IRCCS, Milan, Italy

Present affiliations The present affiliation of Lukas M Weber is: Department of Biostatistics, Johns Hopkins Bloomberg School of Public Health, Maryland, Baltimore, USA.

Twitter Bruno Fosso @brunofosso and Monica M Olcina @olcina_mm

Acknowledgements The authors thank Graeme Murray, Leslie Samuel, Dion G Morton and Nicholas P West for provision of the S:CORT cohorts of Grampian and Foxtrot and to all the patients and their families who gave consent to further research on their samples. S:CORT was funded by the Medical Research Council and Cancer Research UK. The authors also thank Riyue 'Sunny' Bao for discussion.

Contributors SG conceived the study and the experimental setup, performed and analyzed the experiments, wrote the manuscript with input from all authors and is responsible for the overall content of this manuscript; CK performed the experiments and the data analysis and wrote the manuscript; LMW, MDR, and GH performed the analysis of RNA-Seq and mass cytometry data; BF and MM performed the microbiota sequencing and analysis; MMO and ED performed the analysis on human datasets; KM assisted with the mouse experiments; and SEA gave critical input for microbiota experiments and interpretation.

Funding This work was supported by 'Lenino Fontana and Maria Lionello' AIRC fellowship, Umberto Veronesi fellowship, ACS-IRG, and NIH P20GM130457 and NIH R01CA258882-01A1 to SG. The S:CORT consortium is a Medical Research Council (MRC)-stratified medicine consortium jointly funded by the MRC and CRUK (UKRI grant number MR/M016587/1). MMO is funded by the MRC (MC_UU_00001/10). ED is supported by the S:CORT Consortium funded by a grant from the MRC and Cancer Research UK.

Competing interests None declared.

Patient consent for publication Not applicable.

Ethics approval This study involves human subjects, and all samples were obtained following individual informed consent and ethical approval by the National Research Ethics Service in the UK (ref 15/EE/0241). The subjects gave informed consent to participate in the study before taking part. All animal experiments were performed following the guidelines established in the Principles of Laboratory Animal Care (directive 86/609/EEC) and approved by the Italian Ministry of Health and under approved protocols by the Institutional Animal Care and Use Committee at MUSC (IACUC-2017-00165; IACUC-2020-01022).

Provenance and peer review Not commissioned; externally peer reviewed.

Data availability statement Data are available in a public, open access repository. Raw RNA-Seq data have been deposited at ArrayExpress under the accession number E-MTAB-8500.

Supplemental material This content has been supplied by the author(s). It has not been vetted by BMJ Publishing Group Limited (BMJ) and may not have been peer-reviewed. Any opinions or recommendations discussed are solely those of the author(s) and are not endorsed by BMJ. BMJ disclaims all liability and responsibility arising from any reliance placed on the content. Where the content includes any translated material, BMJ does not warrant the accuracy and reliability of the translations (including but not limited to local regulations, clinical guidelines, terminology, drug names and drug dosages), and is not responsible for any error and/or omissions arising from translation and adaptation or otherwise.

Open access This is an open access article distributed in accordance with the Creative Commons Attribution Non Commercial (CC BY-NC 4.0) license, which permits others to distribute, remix, adapt, build upon this work non-commercially, and license their derivative works on different terms, provided the original work is properly cited, appropriate credit is given, any changes made indicated, and the use is non-commercial. See <http://creativecommons.org/licenses/by-nc/4.0/>.

ORCID iDs

Marinella Marzano <http://orcid.org/0000-0002-9996-8817>

Enric Domingo <http://orcid.org/0000-0003-4390-8767>

Silvia Guglietta <http://orcid.org/0000-0001-9998-5716>

REFERENCES

- Herrinton LJ, Liu L, Levin TR, *et al.* Incidence and mortality of colorectal adenocarcinoma in persons with inflammatory bowel disease from 1998 to 2010. *Gastroenterology* 2012;143:382–9.
- Klumper L. Cytokines, inflammation and colon cancer. *Curr Cancer Drug Targets* 2011;11:451–64.
- Terzić J, Grivennikov S, Karin E, *et al.* Inflammation and colon cancer. *Gastroenterology* 2010;138:2101–14.
- Buckowitz A, Knaebel H-P, Benner A, *et al.* Microsatellite instability in colorectal cancer is associated with local lymphocyte infiltration and low frequency of distant metastases. *Br J Cancer* 2005;92:1746–53.
- Le DT, Uram JN, Wang H, *et al.* PD-1 blockade in tumors with mismatch-repair deficiency. *N Engl J Med* 2015;372:2509–20.
- Overman MJ, McDermott R, Leach JL, *et al.* Nivolumab in patients with metastatic DNA mismatch repair-deficient or microsatellite instability-high colorectal cancer (CheckMate 142): an open-label, multicentre, phase 2 study. *Lancet Oncol* 2017;18:1182–91.
- Lichtenstern CR, Ngu RK, Shalpour S, *et al.* Immunotherapy, inflammation and colorectal cancer. *Cells* 2020;9. doi:10.3390/cells9030618. [Epub ahead of print: 04 03 2020].
- Overman MJ, Lonardi S, Wong KYM, *et al.* Durable clinical benefit with nivolumab plus ipilimumab in DNA mismatch Repair-Deficient/ Microsatellite Instability-High metastatic colorectal cancer. *J Clin Oncol* 2018;36:773–9.
- Pagès F, Mlecnik B, Marliot F, *et al.* International validation of the consensus immunoscore for the classification of colon cancer: a prognostic and accuracy study. *Lancet* 2018;391:2128–39.
- Saleh M, Trinchieri G. Innate immune mechanisms of colitis and colitis-associated colorectal cancer. *Nat Rev Immunol* 2011;11:9–20.
- Arbore G, West EE, Spolski R, *et al.* T helper 1 immunity requires complement-driven NLRP3 inflammasome activity in CD4⁺ T cells. *Science* 2016;352:aad1210.
- Hajishengallis G, Lambris JD. Crosstalk pathways between Toll-like receptors and the complement system. *Trends Immunol* 2010;31:154–63.
- Guglietta S, Chiavelli A, Zagato E, *et al.* Coagulation induced by C3aR-dependent NETosis drives protumorigenic neutrophils during small intestinal tumorigenesis. *Nat Commun* 2016;7:11037.
- Wu MCL, Brennan FH, Lynch JPL, *et al.* The receptor for complement component C3a mediates protection from intestinal ischemia-reperfusion injuries by inhibiting neutrophil mobilization. *Proc Natl Acad Sci U S A* 2013;110:9439–44.
- Kilkenny C, Browne WJ, Cuthill IC, *et al.* Improving bioscience research reporting: the ARRIVE guidelines for reporting animal research. *PLoS Biol* 2010;8:e1000412.
- Neufert C, Becker C, Neurath MF. An inducible mouse model of colon carcinogenesis for the analysis of sporadic and inflammation-driven tumor progression. *Nat Protoc* 2007;2:1998–2004.
- Lefrançois L, Lycke N. Isolation of mouse small intestinal intraepithelial lymphocytes, Peyer's patch, and lamina propria cells. *Curr Protoc Immunol* 2001;Chapter 3:19.
- Manzari C, Chiara M, Costanza A, *et al.* Draft genome sequence of *Sphingobium* sp. strain BA1, resistant to kanamycin and nickel ions. *FEMS Microbiol Lett* 2014;361:8–9.
- Fosso B, Santamaria M, Marzano M, *et al.* BioMaS: a modular pipeline for bioinformatic analysis of metagenomic amplicons. *BMC Bioinformatics* 2015;16:203.
- Huber W, Carey VJ, Gentleman R, *et al.* Orchestrating high-throughput genomic analysis with Bioconductor. *Nat Methods* 2015;12:115–21.
- Dobin A, Davis CA, Schlesinger F, *et al.* STAR: ultrafast universal RNA-seq aligner. *Bioinformatics* 2013;29:15–21.
- Robinson MD, McCarthy DJ, Smyth GK. edgeR: a Bioconductor package for differential expression analysis of digital gene expression data. *Bioinformatics* 2010;26:139–40.
- McCarthy DJ, Chen Y, Smyth GK. Differential expression analysis of multifactor RNA-Seq experiments with respect to biological variation. *Nucleic Acids Res* 2012;40:4288–97.
- Wu D, Smyth GK. Camera: a competitive gene set test accounting for inter-gene correlation. *Nucleic Acids Res* 2012;40:e133.
- Huang W-Y, Hsu S-D, Huang H-Y, *et al.* MethHC: a database of DNA methylation and gene expression in human cancer. *Nucleic Acids Res* 2015;43:D856–61.
- Mei HE, Leipold MD, Schulz AR, *et al.* Barcoding of live human peripheral blood mononuclear cells for multiplexed mass cytometry. *J Immunol* 2015;194:2022–31.
- Lai L, Ong R, Li J, *et al.* A CD45-based barcoding approach to multiplex mass-cytometry (CyTOF). *Cytometry A* 2015;87:369–74.
- Finck R, Simonds EF, Jager A, *et al.* Normalization of mass cytometry data with bead standards. *Cytometry A* 2013;83:483–94.

- 29 Olcina MM, Balanis NG, Kim RK, *et al.* Mutations in an innate immunity pathway are associated with poor overall survival outcomes and hypoxic signaling in cancer. *Cell Rep* 2018;25:3721–32.
- 30 Tse JWT, Jenkins LJ, Chionh F, *et al.* Aberrant DNA methylation in colorectal cancer: what should we target? *Trends Cancer* 2017;3:698–712.
- 31 Irizarry RA, Ladd-Acosta C, Wen B, *et al.* The human colon cancer methylome shows similar hypo- and hypermethylation at conserved tissue-specific CpG island shores. *Nat Genet* 2009;41:178–86.
- 32 Jung G, Hernández-Illán E, Moreira L, *et al.* Epigenetics of colorectal cancer: biomarker and therapeutic potential. *Nat Rev Gastroenterol Hepatol* 2020;17:111–30.
- 33 Elvington M, Schepp-Berglind J, Tomlinson S. Regulation of the alternative pathway of complement modulates injury and immunity in a chronic model of dextran sulphate sodium-induced colitis. *Clin Exp Immunol* 2015;179:500–8.
- 34 Munkholm P. Review article: the incidence and prevalence of colorectal cancer in inflammatory bowel disease. *Aliment Pharmacol Ther* 2003;18 Suppl 2:1–5.
- 35 Rowan AJ, Lamlum H, Ilyas M, *et al.* APC mutations in sporadic colorectal tumors: A mutational "hotspot" and interdependence of the "two hits". *Proc Natl Acad Sci U S A* 2000;97:3352–7.
- 36 Fodde R, Kuipers J, Rosenberg C, *et al.* Mutations in the APC tumour suppressor gene cause chromosomal instability. *Nat Cell Biol* 2001;3:433–8.
- 37 Dejea CM, Fathi P, Craig JM, *et al.* Patients with familial adenomatous polyposis harbor colonic biofilms containing tumorigenic bacteria. *Science* 2018;359:592–7.
- 38 Tilg H, Adolph TE, Gerner RR, *et al.* The intestinal microbiota in colorectal cancer. *Cancer Cell* 2018;33:954–64.
- 39 Wu S, Rhee K-J, Albesiano E, *et al.* A human colonic commensal promotes colon tumorigenesis via activation of T helper type 17 T cell responses. *Nat Med* 2009;15:1016–22.
- 40 Ahn J, Sinha R, Pei Z, *et al.* Human gut microbiome and risk for colorectal cancer. *J Natl Cancer Inst* 2013;105:1907–11.
- 41 Sobhani I, Tap J, Roudot-Thoraval F, *et al.* Microbial dysbiosis in colorectal cancer (CRC) patients. *PLoS One* 2011;6:e16393.
- 42 Gao Z, Guo B, Gao R, *et al.* Microbiota disbiosis is associated with colorectal cancer. *Front Microbiol* 2015;6:20.
- 43 Xiao Q, Wu J, Wang W-J, *et al.* DKK2 imparts tumor immunity evasion through β -catenin-independent suppression of cytotoxic immune-cell activation. *Nat Med* 2018;24:262–70.
- 44 Cerami E, Gao J, Dogrusoz U, *et al.* The cBio cancer genomics portal: an open platform for exploring multidimensional cancer genomics data. *Cancer Discov* 2012;2:401–4.
- 45 Gao J, Aksoy BA, Dogrusoz U, *et al.* Integrative analysis of complex cancer genomics and clinical profiles using the cBioPortal. *Sci Signal* 2013;6:pl1.
- 46 Kleeman SO, Koelzer VH, Jones HJ, *et al.* Exploiting differential Wnt target gene expression to generate a molecular biomarker for colorectal cancer stratification. *Gut* 2020;69:1092–103.
- 47 Sirinukunwattana K, Domingo E, Richman SD, *et al.* Image-based consensus molecular subtype (imCMS) classification of colorectal cancer using deep learning. *Gut* 2021;70:544–54.
- 48 Guo L, Wang C, Qiu X, *et al.* Colorectal cancer immune infiltrates: significance in patient prognosis and immunotherapeutic efficacy. *Front Immunol* 2020;11:1052.
- 49 Probst HC, McCoy K, Okazaki T, *et al.* Resting dendritic cells induce peripheral CD8⁺ T cell tolerance through PD-1 and CTLA-4. *Nat Immunol* 2005;6:280–6.
- 50 Krieg C, Nowicka M, Guglietta S, *et al.* High-dimensional single-cell analysis predicts response to anti-PD-1 immunotherapy. *Nat Med* 2018;24:144–53.
- 51 de Vries NL, van Unen V, Ijsselssteijn ME, *et al.* High-dimensional cytometric analysis of colorectal cancer reveals novel mediators of antitumour immunity. *Gut* 2020;69:691–703.
- 52 Shalapour S, Karin M. Immunity, inflammation, and cancer: an eternal fight between good and evil. *J Clin Invest* 2015;125:3347–55.
- 53 Moser AR, Pitot HC, Dove WF. A dominant mutation that predisposes to multiple intestinal neoplasia in the mouse. *Science* 1990;247:322–4.
- 54 Su LK, Kinzler KW, Vogelstein B, *et al.* Multiple intestinal neoplasia caused by a mutation in the murine homolog of the APC gene. *Science* 1992;256:668–70.
- 55 Hinoi T, Akyol A, Theisen BK, *et al.* Mouse model of colonic adenoma-carcinoma progression based on somatic APC inactivation. *Cancer Res* 2007;67:9721–30.
- 56 Souris JS, Zhang HJ, Dougherty U, *et al.* A novel mouse model of sporadic colon cancer induced by combination of conditional APC genes and chemical carcinogen in the absence of Cre recombinase. *Carcinogenesis* 2019;40:1376–86.
- 57 Becher B, Waisman A, Lu L-F. Conditional gene-targeting in mice: problems and solutions. *Immunity* 2018;48:835–6.
- 58 Grivennikov SI, Wang K, Mucida D, *et al.* Adenoma-linked barrier defects and microbial products drive IL-23/IL-17-mediated tumour growth. *Nature* 2012;491:254–8.
- 59 Wang K, Kim MK, Di Caro G, *et al.* Interleukin-17 receptor a signaling in transformed enterocytes promotes early colorectal tumorigenesis. *Immunity* 2014;41:1052–63.
- 60 Amicarella F, Muraro MG, Hirt C, *et al.* Dual role of tumour-infiltrating T helper 17 cells in human colorectal cancer. *Gut* 2017;66:692–704.
- 61 Korn T, Bettelli E, Gao W, *et al.* IL-21 initiates an alternative pathway to induce proinflammatory T(H)17 cells. *Nature* 2007;448:484–7.
- 62 Nurieva R, Yang XO, Martinez G, *et al.* Essential autocrine regulation by IL-21 in the generation of inflammatory T cells. *Nature* 2007;448:480–3.
- 63 Skak K, Kragh M, Hausman D, *et al.* Interleukin 21: combination strategies for cancer therapy. *Nat Rev Drug Discov* 2008;7:231–40.
- 64 Bhatia S, Curti B, Ernstoff MS, *et al.* Recombinant interleukin-21 plus sorafenib for metastatic renal cell carcinoma: a phase 1/2 study. *J Immunother Cancer* 2014;2:2.
- 65 Coquet JM, Skak K, Davis ID, *et al.* IL-21 modulates activation of NKT cells in patients with stage IV malignant melanoma. *Clin Transl Immunology* 2013;2:e6.
- 66 Steele N, Anthony A, Saunders M, *et al.* A phase 1 trial of recombinant human IL-21 in combination with cetuximab in patients with metastatic colorectal cancer. *Br J Cancer* 2012;106:793–8.
- 67 Shapiro M, Nandi B, Gonzalez G, *et al.* Deficiency of the immunostimulatory cytokine IL-21 promotes intestinal neoplasia via dysregulation of the Th1/Th17 axis. *Oncimmunology* 2017;6:e1261776.
- 68 Jauch D, Martin M, Schiechl G, *et al.* Interleukin 21 controls tumour growth and tumour immunosurveillance in colitis-associated tumorigenesis in mice. *Gut* 2011;60:1678–86.
- 69 Kesselring R, Jauch D, Fichtner-Feigl S. Interleukin 21 impairs tumor immunosurveillance of colitis-associated colorectal cancer. *Oncimmunology* 2012;1:537–8.
- 70 Stolfi C, Rizzo A, Franzè E, *et al.* Involvement of interleukin-21 in the regulation of colitis-associated colon cancer. *J Exp Med* 2011;208:2279–90.
- 71 De Simone V, Ronchetti G, Franzè E, *et al.* Interleukin-21 sustains inflammatory signals that contribute to sporadic colon tumorigenesis. *Oncotarget* 2015;6:9908–23.
- 72 Grasso CS, Giannakis M, Wells DK, *et al.* Genetic mechanisms of immune evasion in colorectal cancer. *Cancer Discov* 2018;8:730–49.
- 73 DeStefano Shields CE, White JR, Chung L, *et al.* Bacterial-Driven Inflammation and Mutant BRAF Expression Combine to Promote Murine Colon Tumorigenesis That Is Sensitive to Immune Checkpoint Therapy. *Cancer Discov* 2021;11:1792–807.
- 74 Del Poggetto E, Ho I-L, Balestrieri C, *et al.* Epithelial memory of inflammation limits tissue damage while promoting pancreatic tumorigenesis. *Science* 2021;373:eabj0486.
- 75 Martin TD, Patel RS, Cook DR, *et al.* The adaptive immune system is a major driver of selection for tumor suppressor gene inactivation. *Science* 2021;373:1327–35.
- 76 Ajona D, Ortiz-Espinosa S, Moreno H, *et al.* A combined PD-1/C5a blockade synergistically protects against lung cancer growth and metastasis. *Cancer Discov* 2017;7:694–703.
- 77 Wang Y, Sun S-N, Liu Q, *et al.* Autocrine complement inhibits IL10-Dependent T-cell-mediated antitumor immunity to promote tumor progression. *Cancer Discov* 2016;6:1022–35.
- 78 Liu X, Hogg GD, DeNardo DG. Rethinking immune checkpoint blockade: 'Beyond the T cell'. *J Immunother Cancer* 2021;9:e001460.
- 79 Dhupkar P, Gordon N, Stewart J, *et al.* Anti-PD-1 therapy redirects macrophages from an M2 to an M1 phenotype inducing regression of os lung metastases. *Cancer Med* 2018;7:2654–64.
- 80 Kirchberger S, Royston DJ, Boulard O, *et al.* Innate lymphoid cells sustain colon cancer through production of interleukin-22 in a mouse model. *J Exp Med* 2013;210:917–31.
- 81 Huber S, Gagliani N, Zenewicz LA, *et al.* IL-22BP is regulated by the inflammasome and modulates tumorigenesis in the intestine. *Nature* 2012;491:259–63.
- 82 Pelczar P, Witkowski M, Perez LG, *et al.* A pathogenic role for T cell-derived IL-22BP in inflammatory bowel disease. *Science* 2016;354:358–62.
- 83 Tjalsma H, Boleij A, Marchesi JR, *et al.* A bacterial driver-passenger model for colorectal cancer: beyond the usual suspects. *Nat Rev Microbiol* 2012;10:575–82.

SUPPLEMENTARY INFORMATION

FIGURES

Supplementary figure 1. Stage-related C3aR expression in CRC patients.

C3aR expression in stage I to stage IV CRC patients from the TCGA dataset. Significance was calculated using 1-way Anova with Bonferroni post-test (** $p < 0.01$).

Supplementary figure 2. Loss of C3aR exacerbate inflammation and tumor development in inflammation-driven CRC.

(A) Weight loss in WT and C3aR^{-/-} mice treated with AOM/DSS. (B) The total number of tumors in WT and C3aR^{-/-} mice colon. (C) Single tumor diameters in WT and C3aR^{-/-} mice were measured with a sliding caliper and assigned to the groups $< 2\text{mm}$ or $> 2\text{mm}$ and used to calculate (D) tumor load. Display of total numbers of dendritic cells and macrophages, Tregs (CD3⁺ CD4⁺ CD25⁺ FoxP3⁺), Th1 (CD3⁺CD4⁺ IFN- γ ⁺) cells, Th17 (CD3⁺CD4⁺ IL-17A⁺) cells, Th1/Th17 (CD3⁺CD4⁺ IFN- γ +IL-17A⁺) cells and Tc (CD8⁺IFN γ ⁺) in mLN and in the tumors (H-J) by flow cytometry. Results are pooled from two independent experiments with a minimum of 11 mice/group in A-D and five mice/group in E-J. Significance was calculated in A, B and D using t-test; 2-way ANOVA with Bonferroni post-test was used in panel C and E-J (* $p < 0.05$; ** $p < 0.01$; *** $p < 0.001$).

Supplementary figure 3. Loss of C3aR expression does not significantly impact the functional and phenotypic composition of mLN-infiltrating lymphocytes.

Single cell suspensions from mLN of WT, APC^{Min/+}, APC^{Min/+}/C3aR^{-/-} and C3aR^{-/-} mice were analyzed by FACS and total number of (A) CD4⁺T cells, (B) Th17 cells, (C) Th1 cells, (D) Th1/Th17 cells, (E) CD8⁺T cells, (F) Tc cells were obtained. 9 animals/group were used, and

significance was calculated using 1-way Anova with Bonferroni post-test (** $p < 0.01$; **** $p > 0.0001$).

Supplementary figure 4. Transplantation of the APC^{Min/+}/C3aR^{-/-} microbiota does not affect the number of tumors in the small intestine (SI) and the functional profile of mLN-infiltrating lymphocytes.

5-week-old APC^{Min/+} mice (recipients) were treated for 1 week with broad spectrum antibiotics. 48 h after antibiotics treatment, the recipient mice were transplanted via oral gavage with the gut microbiota of 12-week-old APC^{Min/+} or APC^{Min/+}/C3aR^{-/-} mice (donors) for 3 consecutive days and again once/week for 7 weeks. (A) Total tumor count in the SI and (B) in the different portions of the SI: duodenum (D), jejunum (J) and ileum (I) of recipient mice. (C-H) Flow cytometry analysis of mLN infiltrating lymphocytes showing in (C) total CD4⁺T cells, (D) Th17 cells, (E) Th1 cells, (F) Th1/Th17 cells, (G) CD8⁺ T cells and (H) Tc cells. Shown are results of 2 independent experiments with 11 mice/group. Significance was calculated in A and B using 1-way Anova and 2-way Anova respectively with Bonferroni post-test and in C-H using unpaired T test (** $p < 0.01$; *** $p < 0.001$; **** $p < 0.0001$).

Supplementary figure 5. Impact of C3aR on tumor- and mucus-associated microbiota species.

Bacterial DNA was extracted from colon tumors and mucus of 12-week-old APC^{Min/+} and APC^{Min/+}/C3aR^{-/-} mice and metagenomic analysis was performed. Doughnut charts showing the bacterial composition of tumors (A) and mucus (B) in 12-week-old APC^{Min/+} and APC^{Min/+}/C3aR^{-/-} mice. Significance was calculated in A by DESeq R-package.

Supplementary figure 6. Differential gene expression analysis in distal colon of APC^{Min/+}, APC^{Min/+}/C3aR^{-/-}, C3aR^{-/-} and WT mice.

Summary plot showing the number of significantly differentially expressed genes in distal colons of (A) C3aR^{-/-} vs. WT mice (n=4); (B) APC^{Min/+} vs. WT mice; (C) APC^{Min/+}/C3aR^{-/-} vs. C3aR^{-/-} mice; (D) APC^{Min/+}/C3aR^{-/-} vs. WT mice; (E) APC^{Min/+} vs. C3aR^{-/-} mice. The plots display log fold change against log counts per million for each gene with the red points representing significant differentially expressed genes, and the horizontal blue lines indicating a 2-fold increase or decrease in expression. Significance was calculated using the edgeR function `decideTestsDGE` with default p-value adjustment method (Benjamini-Hochberg false discovery rate, FDR), default p-value threshold (0.05), and a custom log fold change threshold of 1 (1 on the log₂ scale, equivalent to a relative change of 2 or 0.5 in non-logarithmic terms).

Supplementary figure 7. Loss of C3aR results in transcriptional up-regulation of innate and adaptive immune pathways in the healthy distal colon of APC^{Min/+}/C3aR^{-/-} mice.

(A) Heatmap from (row-wise z-transformed) log counts per million values, using data from distal colon of indicated mouse strains and all genes that are significant at 5% FDR in at least one contrast. Rows represent genes, and columns represent individual samples. Each row (gene) is z-transformed to have mean zero and standard deviation one. The heatmap also includes column annotation labels indicating the mouse strain for each sample. (B) Visualization of the gene-associated Gene Ontology (GO) biological processes in healthy colon. (C) Volcano plot illustrating the magnitude of fold change for all genes differentially expressed in the distal colon of APC^{Min/+} vs. APC^{Min/+}/C3aR^{-/-} mice (n=4). Representative significantly up-regulated and down-regulated genes belonging to the GO biological processes shown in B are highlighted in yellow. Significance was calculated using the edgeR function `decideTestsDGE` with Benjamini-Hochberg correction for false discovery rate (FDR); a default FDR threshold of 0.05 and a log₂ fold change (log₂FC) threshold of 0.6 were applied.

Supplementary figure 8. Validation of the mass cytometry panel

The antibody panel was validated by solution mass cytometry on fresh cells isolated from WT spleen and colon lamina propria digested with collagenase VIII. For cytokines, the cells were stimulated with PMA/Ionomycin, stained with surface antibodies and then permeabilized to perform the intracellular staining following the procedures described in the material and methods of our manuscript. Metal-tagged antibodies against PE and APC were used to detect IL-17A-PE and IFN- γ -APC, respectively.

Supplementary Figure 9. Small intestinal tumors in APC^{Min/+} and APC^{Min/+}/C3aR^{-/-} mice

Tumor burden in the small intestine of APC^{Min/+} and APC^{Min/+}/C3aR^{-/-} mice from 5 to 24 weeks. Significance was calculated in a by 1-way Anova with Bonferroni post-test (ns= not significant; **p<0.01; **** p<0.0001).

MATERIALS AND METHODS**Animals**

C3aR^{-/-} mice on C57BL/6J background were a kind gift from Dr. Bao Lu and Dr. Carl Atkinson. APC^{Min/+}/C3aR^{-/-} mice were generated by crossing APC^{Min/+} with C3aR^{-/-} mice in our animal facilities. Male and female mice were used throughout the study unless otherwise specified. All experiments were performed during the light cycle. The animals were housed in individually ventilated cages with corn cob bedding. Non littermate mice were co-housed for a minimum of two weeks before performing any intervention.

CRC models

For inflammation-driven CRC, mice were treated 10 mg/Kg of azoxymethane (AOM; Sigma-Aldrich). After 7 days, mice were administered with 1.5% (w/v) DSS (TdB Consultancy) in their drinking water for 1 week followed by 2 weeks of recovery with water. DSS/recovery cycles were

repeated three times as previously described¹. For the spontaneous tumor model APC^{Min/+} and APC^{Min/+}/C3aR^{-/-} mice were euthanized at indicated time points, tumor counted and used for downstream applications.

Flow cytometry and preparation of single cell suspensions

Single cell suspensions were prepared from mLN following standard protocols. Colon lamina propria cells were isolated as previously described with minor modifications². For isolation of tumor-associated immune cells, colon polyps were shaken in PBS, 1% BSA, 10 mM EDTA to remove epithelial cells, and further digested for 30 minutes at 37°C with Collagenase VIII (Sigma-Aldrich) in complete medium with shaking.

For flow cytometry staining, cells were incubated with anti-FcR antibody (clone 24G2) and stained with the following surface antibodies: anti-CD45.2 (clone 104, eBioscience), Ly6G (clone 1A8), CD3 (clone 17A2, eBioscience), Ly6C (clone AL-21), CD11b (clone M1/70), CD4 (clone RM4-5), CD8a (53-6-7), B220 (clone RA3-6B2), I-A/I-E (clone M5/114.15.2), CD11c (clone HL3), F4/80 (MB8, eBioscience), CD103 (clone 2E7), CD25 (clone PC61), anti-IFN- γ (clone XMG1.2), anti-IL-17A (clone TC11-18H10), anti-FoxP3 (clone FJK-16s eBioscience). For cytokine staining, cells were permeabilized with Cytofix/Cytoperm buffer according to manufacturer instructions. For Foxp3 staining the permeabilization was performed using the FoxP3 permeabilization buffer (eBioscience). All antibodies were purchased from BD Pharmingen unless otherwise specified. Samples were acquired with FACSCanto II or Fortessa LSR (BD Bioscience) and analyzed with FlowJo software (TreeStar).

Fecal microbiota transplantation

For fecal microbiota transplantation (FMT), fecal material was obtained from 12-week-old APC^{Min/+} and APC^{Min/+}/C3aR^{-/-} donor mice. Briefly, fecal pellet and cecal contents were harvested

from the mice, dissolved in sterile PBS at 100 mg/ml, passed through a 70- μ m strainer in order to eliminate insoluble debris, and frozen in Columbia broth with 20% glycerol. At the time of administration, aliquots were thawed, centrifuged to eliminate the glycerol-containing medium and resuspended at 100 mg/ml for gavage. This procedure allowed us to use the same material throughout the experiment, thereby avoiding confounding effects due to fecal material coming from different animals. Five-week-old APC^{Min/+} mice were used as FMT recipient. Recipient mice were treated for one week with the broad-spectrum antibiotics in the drinking water, rested for 48 h with water without antibiotics, followed by gavage with 200 μ l /mouse of the previously prepared fecal material for 3 consecutive days in the first week and once a week for the next 6 weeks.

Microbiota profiling

V5-V6 hypervariable regions of bacterial 16S rRNA gene were amplified and processed with a modified version of the Nextera protocol³. The obtained metabarcoding libraries were sequenced by using the MiSeq Illumina platform with a 2x250 paired end (PE) approach. Metagenomic amplicons were analyzed by applying the BioMaS⁴ pipeline as follows: (i) The paired-end reads were merged into consensus sequences using Flash⁵ and subsequently dereplicated as previously described⁶ maintaining the consensus sequence; (ii) The remaining non overlapping PE reads were considered for further analysis only if after the low-quality region trimming (Phred quality cut-off = 25) both read ends were ≥ 50 bp long⁷; Both the merged sequences and the unmerged reads were matched against the RDP (Ribosomal Database Project) database (release 10.29)⁸ by Bowtie2⁹. The mapping data were filtered according to two parameters: identity percentage ($\geq 97\%$) and query coverage ($\geq 70\%$); (iv) Finally, all mapped reads fulfilling the settled filters were taxonomically annotated using the Tango tool¹⁰. Assigned genera were filtered considering as present only the ones for which at least five reads per samples were present. The read counts were

normalized using an approach similar to the RPKM (Reads per kilo-base per million): $\text{normalized count} = \text{assigned reads} / (\text{total assigned reads at the rank level} / 1,000,000)$. Significant differences at the genus and species level were calculated with the DESeq R-package¹¹. A tree representing the phylogenetic relationship between the Amplicon Sequence Variants (ASV) was produced by using the QIIME1 package¹². The rarefaction curves were inferred and plotted by using an in house developed R script relying on the rarefy function of the vegan package. Alpha and Beta diversity analysis were performed using the phyloseq R¹³. In particular, the observed ASVs, the Shannon and the Faith Indexes were used as richness and alpha diversity measures. The weighted and unweighted UniFrac and the Bray-Curtis metrics were used for the Beta diversity inference¹⁴. Difference in the inferred alpha diversity indices were measured by using the Kruskal-Wallis test followed by a pairwise Wilcoxon as post-hoc test (p-values corrected by using the Benjamin-Hochberg procedure). The PERMANOVA test was used to compare groups in beta diversity data, using 999 permutations. To isolate bacterial DNA from mucus scraped from the colon we used the same protocol used to isolate bacterial DNA from the feces. For the isolation of tumor-associated bacteria, tumors were homogenized in sterile phosphate buffered saline solution, centrifuged, and both supernatants and pellets were subjected to depletion of host DNA by using the QIAamp DNA Microbiome kit (Qiagen) before proceeding with bacterial DNA extraction. Sequencing libraries were prepared using the Nextera XT Library Preparation kit (Illumina) following the manufacturer's guidelines and ran on HiSeq 2500 platform (Illumina).

RNA-Seq

For RNASeq analysis, 12-week-old APC^{Min/+}, WT, C3aR^{-/-} and APC^{Min/+}/C3aR^{-/-} mice (4 mice/group) were sacrificed. The proximal (first 3 cm adjacent to the caecum) and distal colon (the final 3.5 cm adjacent to the rectum) and the single tumors were immediately preserved in 2

ml of RNAlater stabilization solution (Qiagen) according to manufacturer instructions and stored at -20°C. For RNA extraction, tumors and colons were homogenized in Trizol (500 µl/50 mg weight), centrifuged at 13000 rpm. The supernatant was loaded on Qiagen Mini Kit columns and treated as indicated in the manufacturer instructions. RNA concentration was quantified by Nanodrop and quality and integrity were evaluated by using a bioanalyzer (Agilent Technologies). Only samples with a RIN>8 were used for downstream applications. Briefly, 1 µg of RNA was used to prepare cDNA with the TruSeq RNA kit following the recommendations for low sample preparation protocol (Illumina). Samples were sequenced on an Illumina MiSeq instrument at a depth of 35x10⁶ reads per sample. Reads in FASTQ format were quantified at the gene level using featureCounts and the count table was delivered to edgeR for the differential expression analysis using the GLM functionality^{15, 16}. GO analysis was conducted to identify DEG at the biologically functional level. The identified DEGs were uploaded to the online software Advaita Bioinformatics to integrate functional genomic annotations. A false discovery rate (FDR) cutoff of 5% and minimum fold change of 1.5 (log2FC=0.6) was applied to determine differential expression.

Analysis of C3aR expression, methylation and correlation with immune cells in patients with CRC

Data on C3aR expression were obtained from the R2 Genomics Analysis and Visualization Platform (<http://r2.amc.nl>) or TCGA database. C3aR expression data were plotted with PRISM (GraphPad Software). Data on C3aR methylation were obtained from the human pan-cancer methylation database (MethHC, <http://methhc.mbc.nctu.edu.tw/php/index.php>)¹⁷.

Spearman and Pearson correlations between C3aR (queried as *c3ar1*) mRNA expression and diverse immune cell populations (assessed by CIBERSORT) were made available for this study

and downloaded through the private S:CORT cBioPortal for 179 colon cancer patients (FOXTROT cohort) and 231 rectal cancer patients. All cases in the S:CORT WS3 Grampian Set (retrospective cohort) were included in the study.

Immune cell populations queried: CIBERSORT: Resting dendritic cells, naïve B-cells, resting and activated NK cells, regulatory T cells, CD8 T-cells, plasma cells, neutrophils, monocytes, M1 and M2 macrophages, CD4 T cells.

Mass cytometry

Mass cytometry antibodies were either labelled in-house using antibody-labelling kits and protocols according to manufacturer's instructions or purchased from Fluidigm. Antibodies were individually titrated and optimized into the final panel before use, ensuring that each parameter was informative.

After barcoding, the composite sample was stained with the cocktail of primary antibodies (Table 1), washed and fixed with 1.6% paraformaldehyde (PFA; Electron Microscopy Sciences) at 4 °C. Fixed cells were permeabilized and resuspended in 400 µl of intracellular antibody mixture (Suppl. Table 1) in permeabilization buffer at 4°C. After washing, samples were incubated with DNA-intercalating solution (Iridium (Sigma) in MaxPar Fix/Perm buffer (Fluidigm) overnight at 4°C. Before the acquisition, the samples were washed twice with MilliQ water. Barcoded composite samples were acquired on a Helios mass cytometer (Fluidigm). Quality control and tuning processes on the Helios are performed daily before acquisition. Data from different days and across acquisition time was normalized by adding five-element beads to the sample immediately before acquisition and using the MATLAB-based normalization software, as described previously¹⁸.

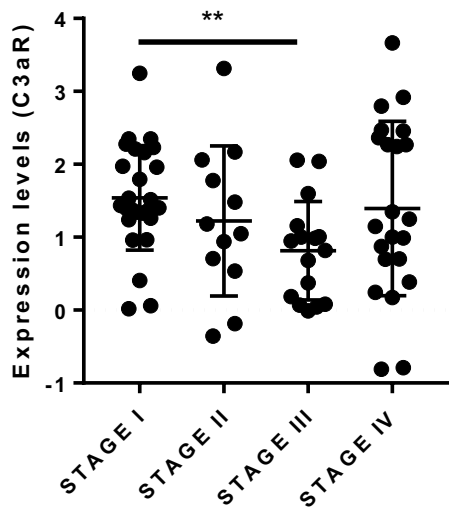
REFERENCES

1. Neufert C, Becker C, Neurath MF. An inducible mouse model of colon carcinogenesis for the analysis of sporadic and inflammation-driven tumor progression. *Nat Protoc* 2007;2:1998-2004.
2. Lefrancois L, Lycke N. Isolation of mouse small intestinal intraepithelial lymphocytes, Peyer's patch, and lamina propria cells. *Curr Protoc Immunol* 2001;Chapter 3:Unit 3 19.
3. Manzari C, Chiara M, Costanza A, et al. Draft genome sequence of *Sphingobium* sp. strain ba1, resistant to kanamycin and nickel ions. *FEMS Microbiol Lett* 2014;361:8-9.
4. Fosso B, Santamaria M, Marzano M, et al. BioMaS: a modular pipeline for Bioinformatic analysis of Metagenomic AmpliconS. *BMC Bioinformatics* 2015;16:203.
5. Magoc T, Salzberg SL. FLASH: fast length adjustment of short reads to improve genome assemblies. *Bioinformatics* 2011;27:2957-63.
6. Edgar RC. Search and clustering orders of magnitude faster than BLAST. *Bioinformatics* 2010;26:2460-1.
7. Mariathasan S, Turley SJ, Nickles D, et al. TGFbeta attenuates tumour response to PD-L1 blockade by contributing to exclusion of T cells. *Nature* 2018;554:544-548.
8. Cole JR, Wang Q, Cardenas E, et al. The Ribosomal Database Project: improved alignments and new tools for rRNA analysis. *Nucleic Acids Res* 2009;37:D141-5.
9. Langmead B, Salzberg SL. Fast gapped-read alignment with Bowtie 2. *Nat Methods* 2012;9:357-9.
10. Alonso-Aleman D, Barre A, Beretta S, et al. Further steps in TANGO: improved taxonomic assignment in metagenomics. *Bioinformatics* 2014;30:17-23.

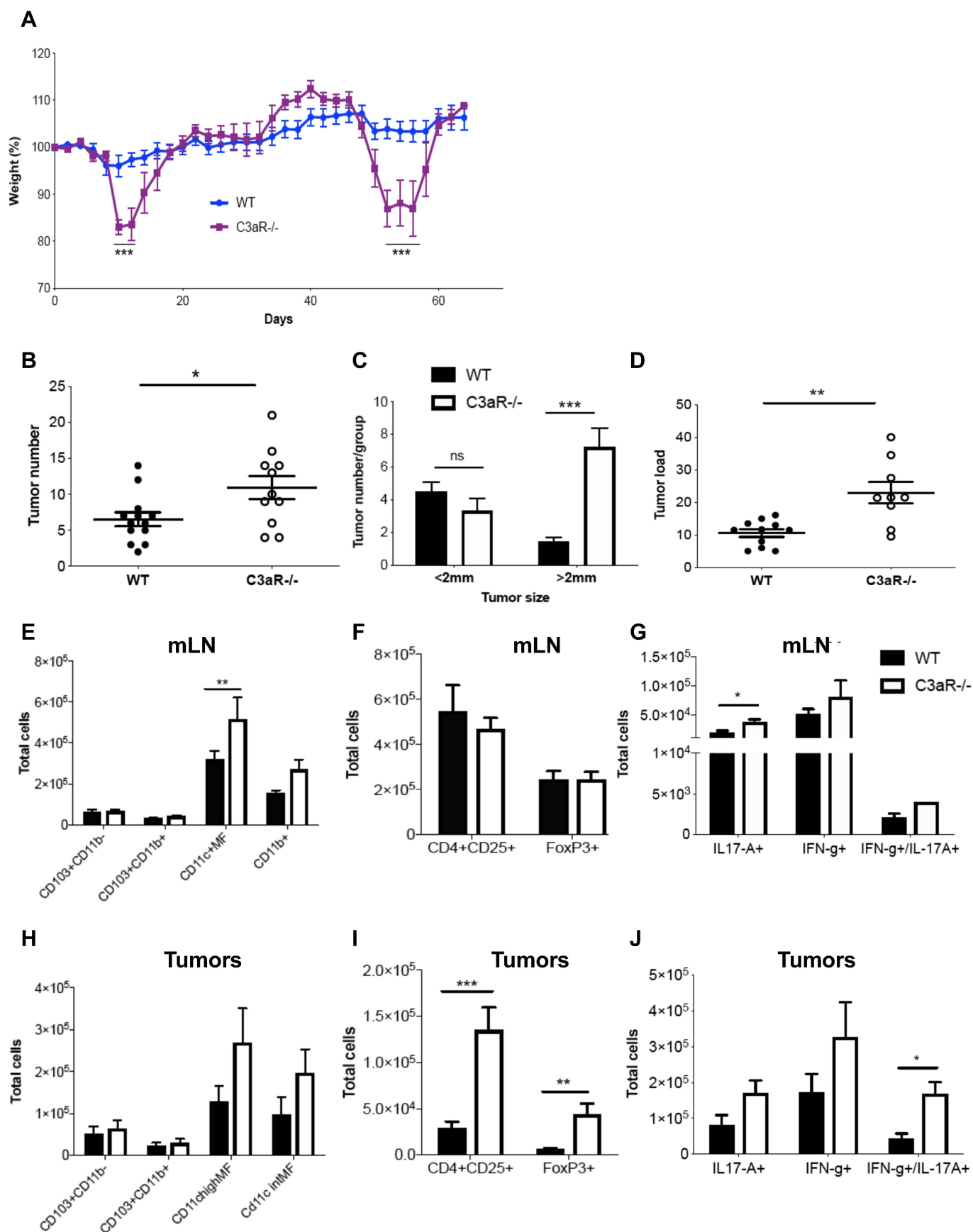
11. Anders S, Huber W. Differential expression analysis for sequence count data. *Genome Biol* 2010;11:R106.
12. Caporaso JG, Kuczynski J, Stombaugh J, et al. QIIME allows analysis of high-throughput community sequencing data. *Nat Methods* 2010;7:335-6.
13. McMurdie PJ, Holmes S. phyloseq: an R package for reproducible interactive analysis and graphics of microbiome census data. *PLoS One* 2013;8:e61217.
14. Chang Q, Luan Y, Sun F. Variance adjusted weighted UniFrac: a powerful beta diversity measure for comparing communities based on phylogeny. *BMC Bioinformatics* 2011;12:118.
15. Liao Y, Smyth GK, Shi W. featureCounts: an efficient general purpose program for assigning sequence reads to genomic features. *Bioinformatics* 2014;30:923-30.
16. McCarthy DJ, Chen Y, Smyth GK. Differential expression analysis of multifactor RNA-Seq experiments with respect to biological variation. *Nucleic Acids Res* 2012;40:4288-97.
17. Huang WY, Hsu SD, Huang HY, et al. MethHC: a database of DNA methylation and gene expression in human cancer. *Nucleic Acids Res* 2015;43:D856-61.
18. Finck R, Simonds EF, Jager A, et al. Normalization of mass cytometry data with bead standards. *Cytometry A* 2013;83:483-94.

Supplementary Figure 1

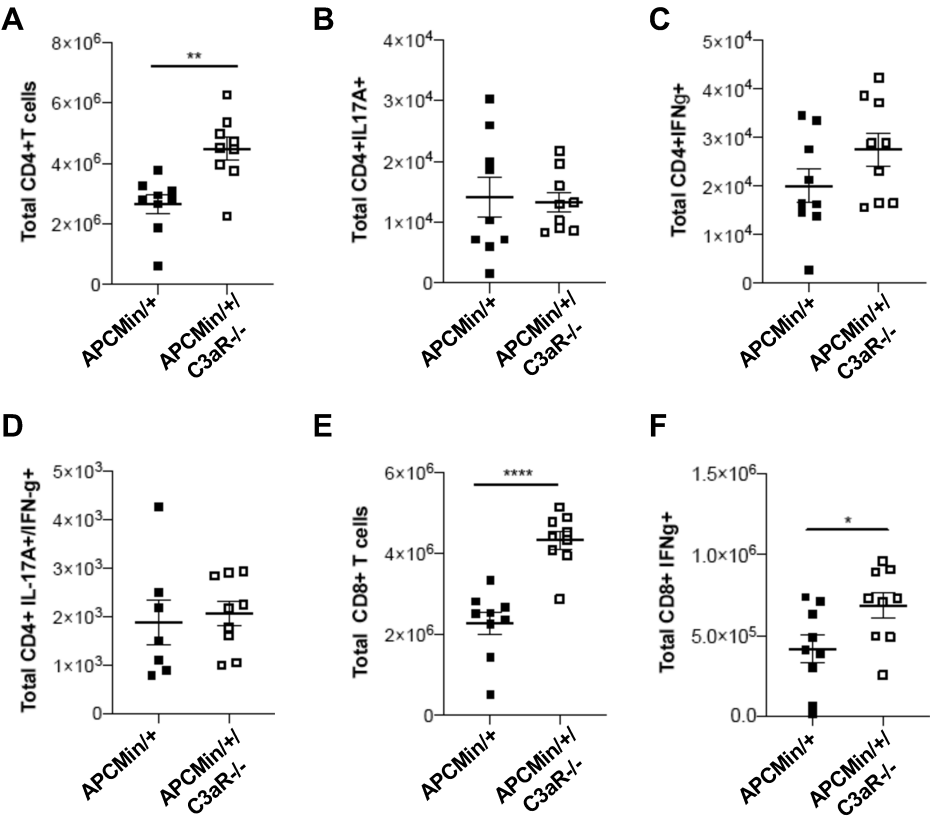
TCGA dataset C3aR expression



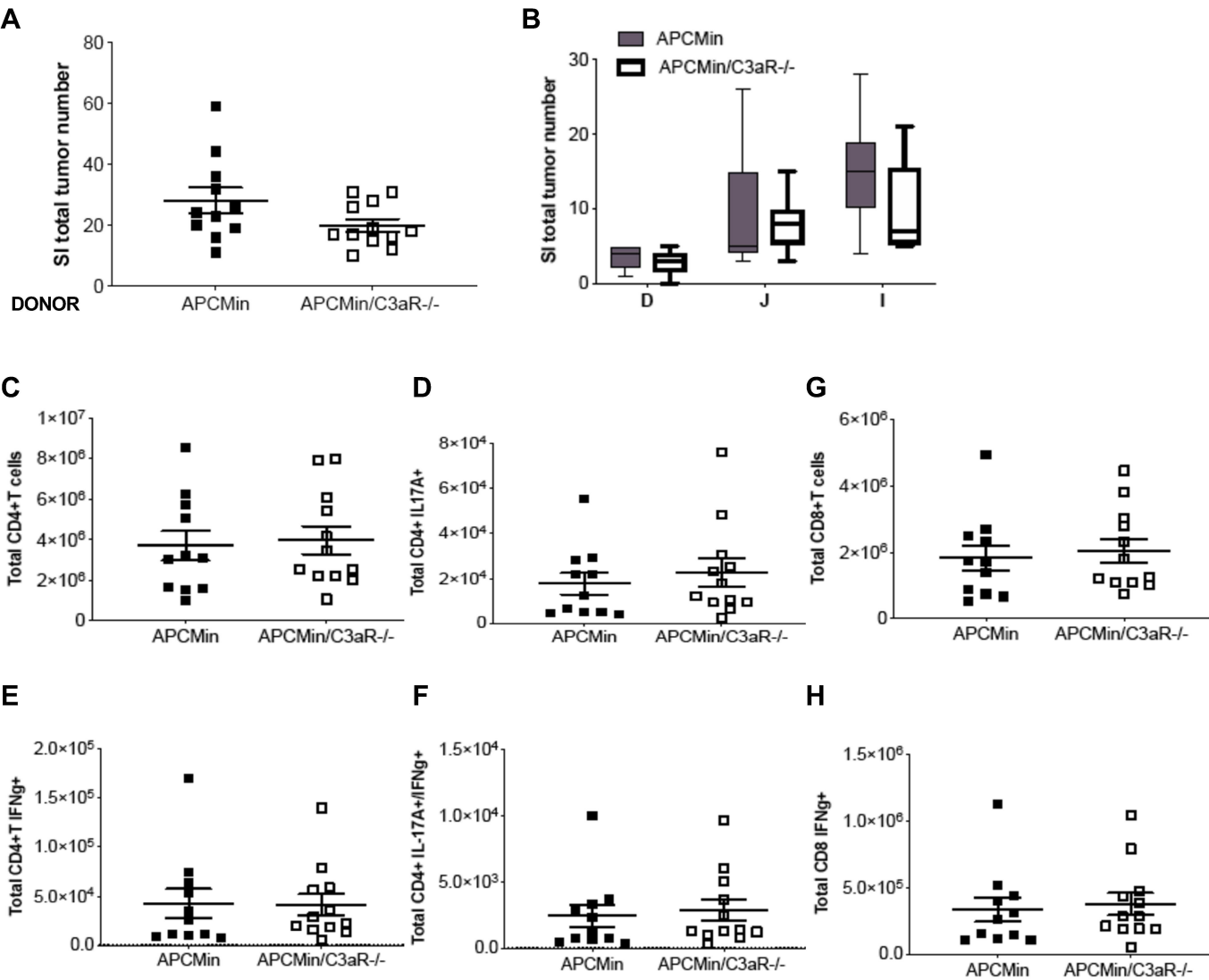
Supplementary Figure 2



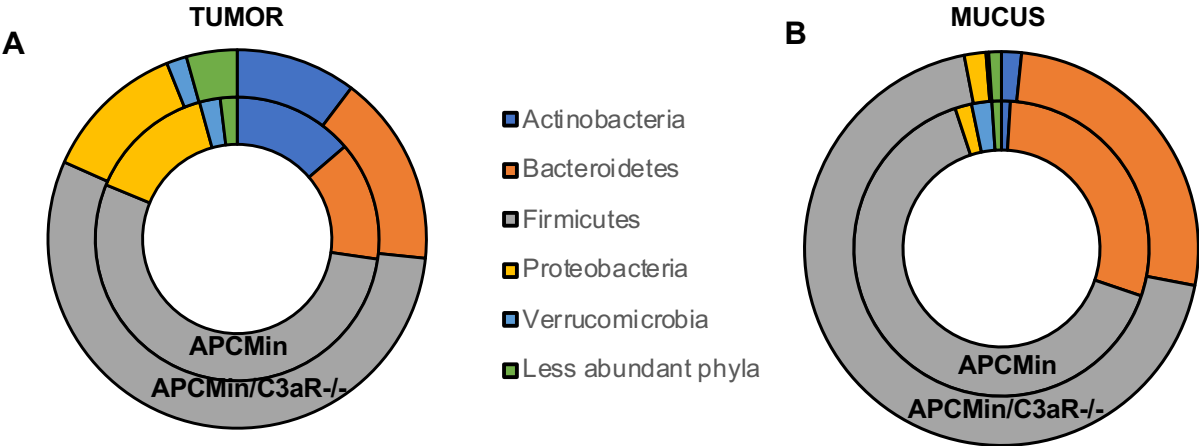
Supplementary Figure 3



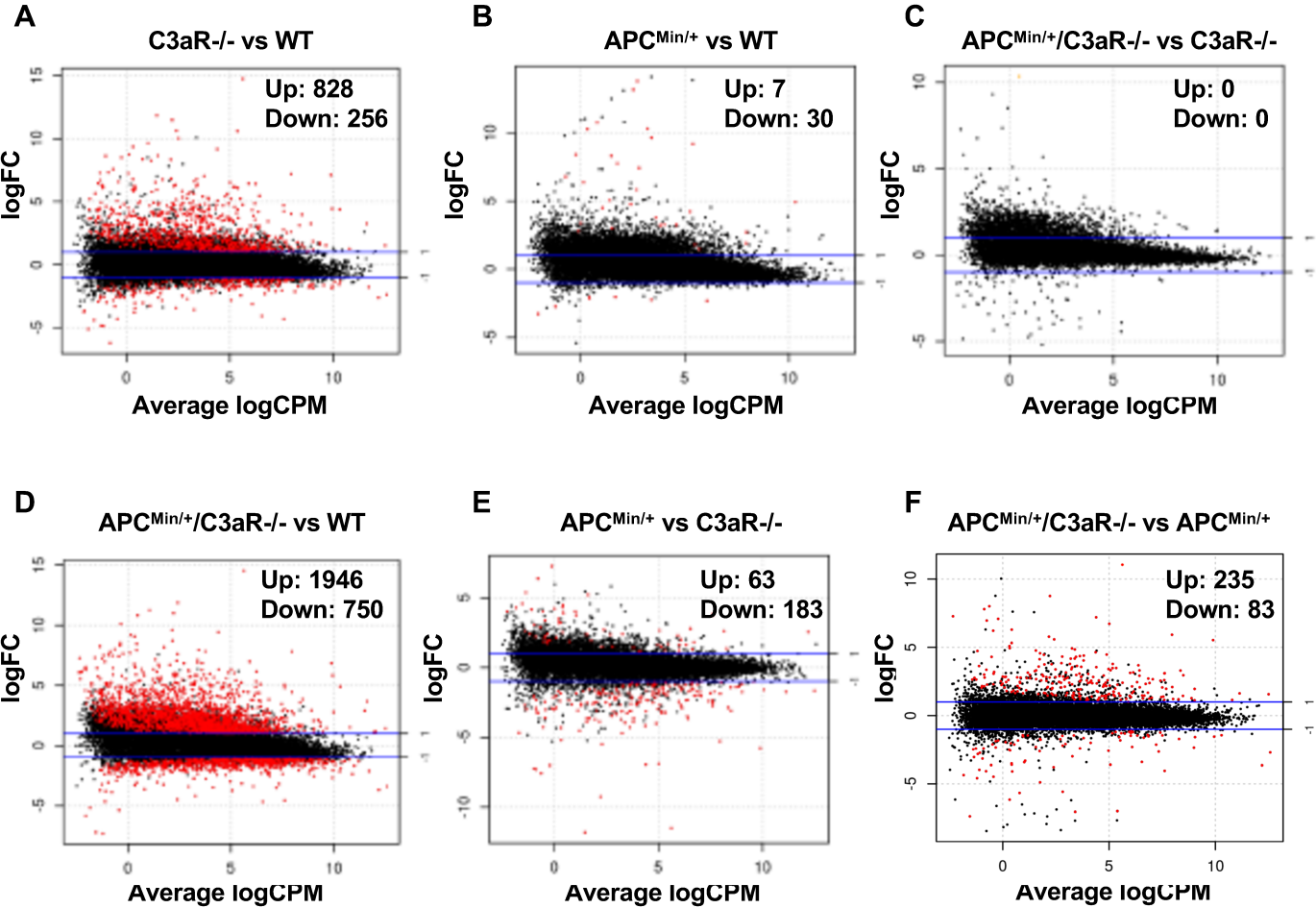
Supplementary Figure 4

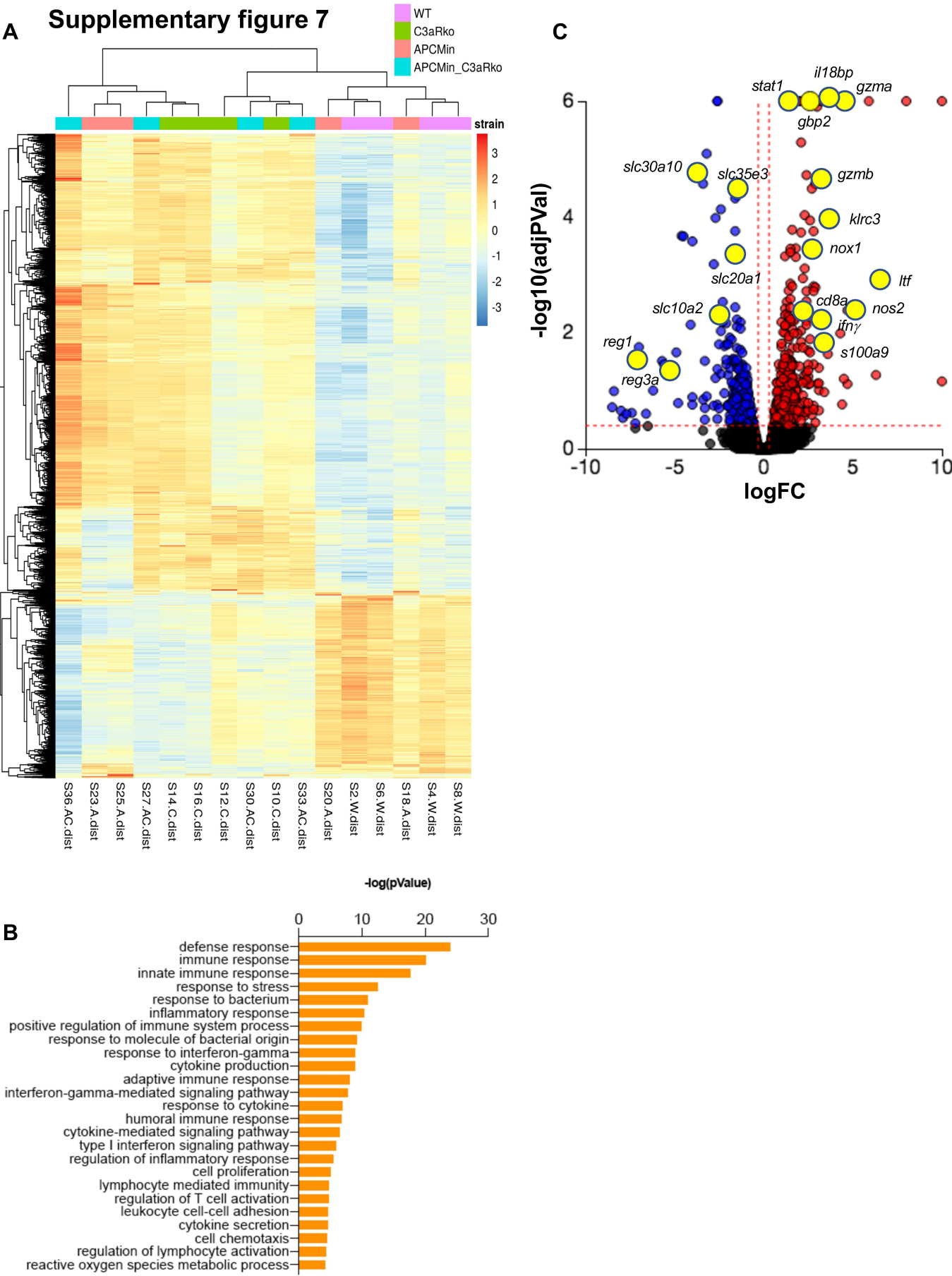


Supplementary figure 5

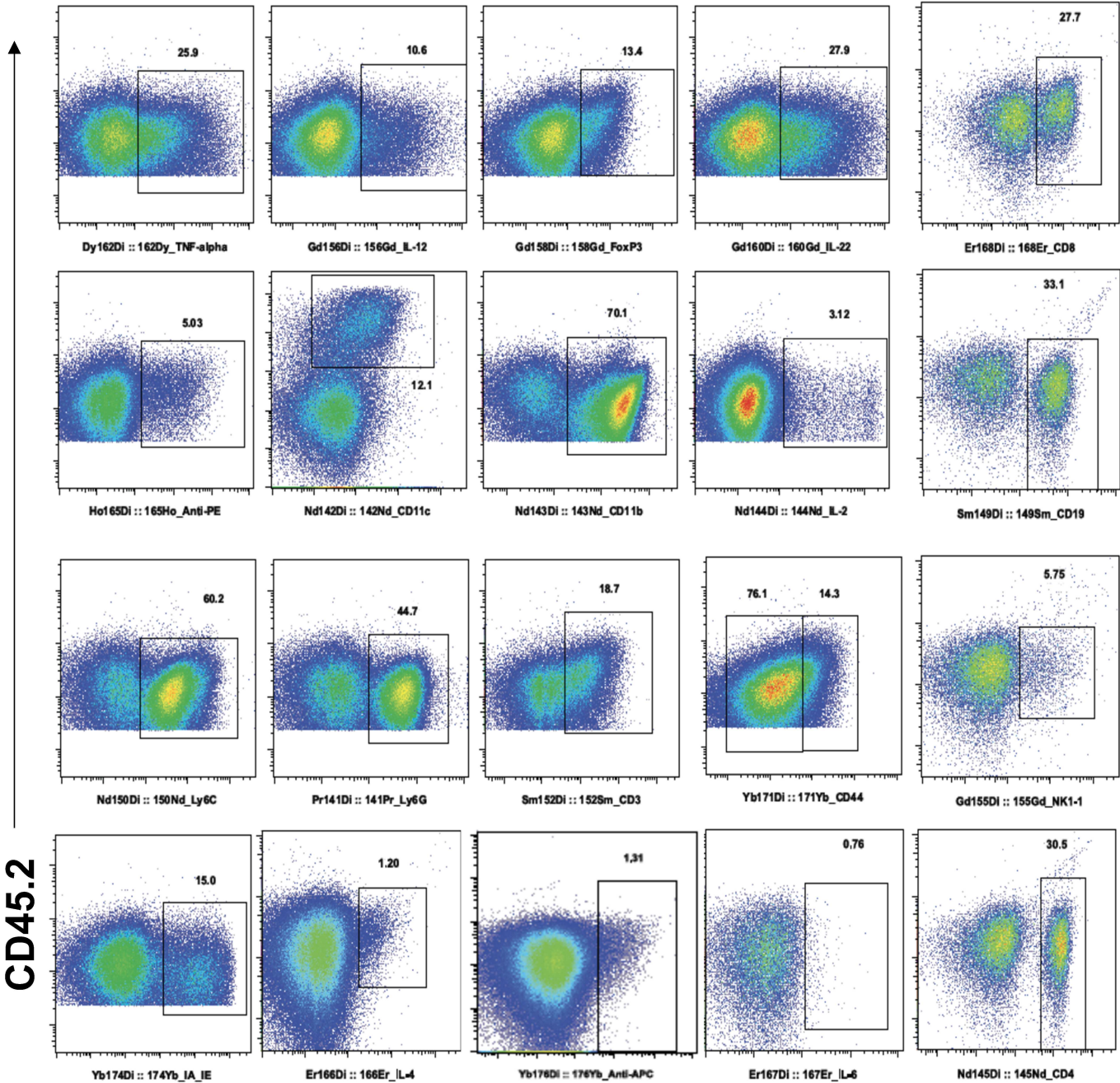


Supplementary Figure 6

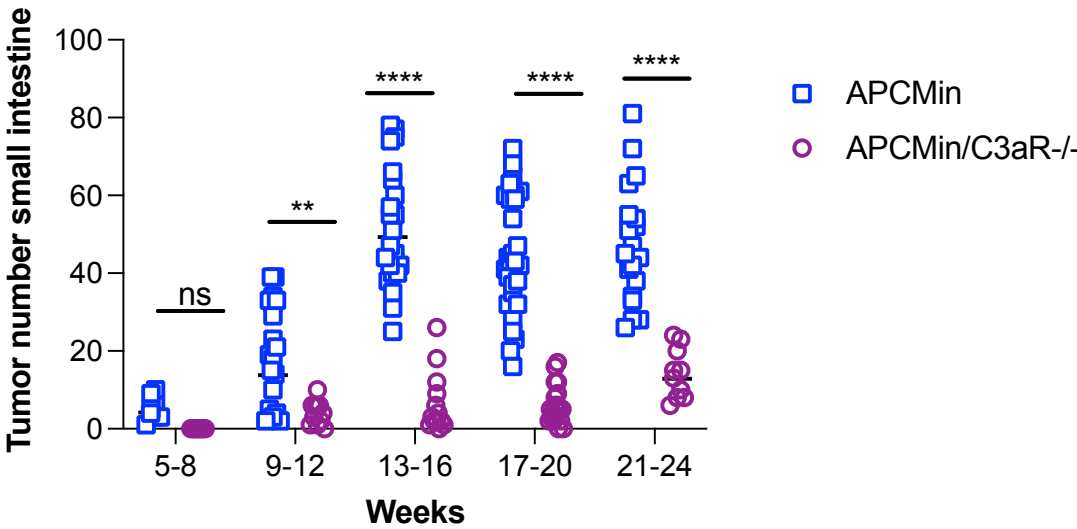




Supplementary figure 8



Supplementary figure 9



CRC	Cibersort		xcell		MCP	
Population name (Cibersort overlap)	R	p-value	R	p-value	R	p-value
Neutrophils	0.33	7.54E-06	0.50024663	1.81E-07	0.532575	1.97E-08
Macrophages_M0	0.33	6.47E-06	0.40681445	3.55E-05		
CD4 resting	0.28	1.47E-04	0.32985489	0.000968796		
Macrophages_M1	0.25	6.12E-04	0.40650321	3.60E-05		
CD8 T cells	-0.3	4.80E-05	-0.28081781	0.00533336	-0.1731918	0.089796
NK cells activated	-0.28	5.78E-08	-0.34205869	0.000605206	-0.0296307	0.773263
Tregs	-0.39056755	8.30E-08	-0.26286856	0.009286821		
CD4 activated	-0.14	5.79E-03	-0.25352064	0.012224454	-0.0542505	0.59766
RC	Cibersort		xcell		MCP	
Population name (Cibersort overlap)	R	p-value	R	p-value	R	p-value
Dendritic_cells_resting	0.347460005	1.00E-07	0.24110623	0.000279053		
Neutrophils	0.313791277	1.75E-06	0.39828579	6.76E-10	0.3459545	1.15E-07
Macrophages_M1	0.25602375	0.0001105	0.61546371	1.23E-24		
NK_cells_resting	0.219192585	0.0009842	0.26347605	6.80E-05		
T_cells_CD4_memory_resting	0.211791833	0.0014671	0.35240985	6.39E-08	0.0617925	0.358383
B_cells_naive	-0.31469163	1.62E-06	-0.20412594	0.002188083	-0.1006696	0.133957
T_cells_CD8	-0.16122597	0.0159581	-0.35656168	4.36E-08	-0.2197795	0.000953
NK_cells_activated	-0.22254934	0.0008176			-0.1690961	0.011433
CRC= colorectal cancer, RC=rectal cancer, R and p-values from Pearson						